SIAM J. SCI. COMPUT.
Vol. 42, No. 6, pp. B1541–B1569

A VARIATIONAL LAGRANGIAN SCHEME FOR A PHASE-FIELD MODEL: A DISCRETE ENERGETIC VARIATIONAL APPROACH*

CHUN LIU† AND YIWEI WANG†

Abstract. In this paper, we propose a variational Lagrangian scheme for a modified phase-field model, which can compute the equilibrium states of the original Allen–Cahn type model. Our discretization is based on a prescribed energy-dissipation law in terms of the flow map. By employing a discrete energetic variational approach, this scheme preserves the variational structure of the continuous energy-dissipation law and is energy stable. Plentiful numerical tests show that, by choosing the initial value properly, our method can compute the desired equilibrium state and capture the thin diffuse interface with a small number of mesh points.

Key words. phase-field model, variational approach, Lagrangian scheme

AMS subject classifications. 65M50, 65M60

DOI. 10.1137/20M1326684

1. Introduction.

Phase-field models, i.e., diffuse interface models, have been a successful tool in studying many problems arising in physics, biology, material science, and image processing [15, 30, 16, 27, 52, 8, 9]. There is a substantial interest in developing efficient numerical methods for phase-field models [41, 32, 31, 23, 36, 56, 58, 19, 68, 55, 54].

From a modeling perspective, phase-field models can be classified into two categories, known as Allen–Cahn type [2] and Cahn–Hilliard type [10]. The Allen–Cahn type models are typical examples of L^2-gradient flows [55], while the Cahn–Hilliard type models, which are concerned with a conserved quantity, are examples of H^1-diffusions [34]. Although numerical methods for both types of phase-field models are well developed [41, 56, 55, 26], most of them are *Eulerian methods*, which solve the equation of the "phase" function φ in a fixed grid [56]. In order to resolve the thin diffuse interface, one must have mesh sizes much smaller than the width of the thin diffuse interface [62, 47, 26], which requires huge computational efforts. This difficulty is often handled by using adaptive mesh techniques [51, 1] or moving mesh approaches [31, 23, 56, 58].

For many real problems modeled by Allen–Cahn type phase-field models, the goal is to find stationary states of the free energy functional. The purpose of this paper is to propose a variational Lagrangian scheme for a modified phase-field model, which can compute equilibrium states of the original Allen–Cahn type model. The approach presented here can be extended to other free energy minimization problems. Compared with Eulerian methods, Lagrangian methods, which are often self-adaptive, have potential advantages for problems involving singularities, sharp interfaces, and free boundaries. Recently, there has been an increasing interest in applying Lagrangian schemes to generalized diffusions, such as the porous medium equation and nonlinear

*Submitted to the journal's Computational Methods in Science and Engineering section March 31, 2020; accepted for publication (in revised form) September 28, 2020; published electronically December 14, 2020.

https://doi.org/10.1137/20M1326684

Funding: This work was partially supported by NSF through grant DMS-1759536.

†Department of Applied Mathematics, Illinois Institute of Technology, Chicago, IL 60616 USA (cliu124@iit.edu, ywang487@iit.edu).

Fokker–Plank equations [13, 67, 14, 39, 12, 45, 11, 42]. However, it is more difficult to construct Lagrangian schemes for L^2-gradient flows. Unlike generalized diffusions, which have natural variational structures on Lagrangian maps [29, 39, 11, 42], the variational structures of L^2-gradient flows are on physical variables defined in Eulerian coordinates. Moreover, as a drawback of all Lagrangian methods, the meshes of Lagrangian solutions may become too skewed, which not only influences the accuracy of the solution but also may result in premature termination of Lagrangian calculations [37].

To overcome these difficulties, we first propose an energy-dissipation law for a phase-field model, given by

$$\frac{\mathrm{d}}{\mathrm{d}t}\int_\Omega W(\varphi,\nabla\varphi)\mathrm{d}\boldsymbol{x} = -\int_\Omega \gamma|\varphi_t|^2 + \nu|\nabla\mathbf{u}|^2\mathrm{d}\boldsymbol{x}, \tag{1.1}$$

where φ is a "phase" function satisfying a transport equation

$$\varphi_t + \nabla\varphi\cdot\mathbf{u} = 0, \tag{1.2}$$

$\mathbf{u}$ is the virtual velocity associated with the Lagrangian map, and $W(\varphi,\nabla\varphi)$ is the free energy density. This model is inspired by phase-field models of a mixture of two incompressible fluids [71, 38, 1]. For $\nu = 0$, this model employs the same energy-dissipation law of Allen–Cahn type models. So one can view (1.1) as a modified Allen–Cahn type model. The additional term in the dissipation part of (1.1) can be viewed as a regularization term on Lagrangian maps, which plays an essential role in calculations. The dissipation part imposes a mechanism to minimize the total free energy in terms of the Lagrangian map for the given initial condition $\varphi_0(\mathbf{X})$.

By employing an energetic variational approach, we can obtain the corresponding PDE of this system, given by

$$\begin{cases} -\nu\Delta\mathbf{u} + \gamma\left(\nabla\varphi\otimes\nabla\varphi\right)\mathbf{u} = -\nabla\cdot\left(\frac{\partial W}{\partial\nabla\varphi}\otimes\nabla\varphi - W(\varphi,\nabla\varphi)\mathrm{I}\right), \\ \varphi_t + \nabla\varphi\cdot\mathbf{u} = 0, \end{cases} \tag{1.3}$$

subject to suitable initial and boundary conditions. Formally, it is straightforward to reformulate (1.1) and (1.3) in terms of a Lagrangian map and its time derivative. Hence, based on the energy-dissipation law (1.1), we can construct a variational-structure-preserving Lagrangian scheme by employing a discrete energetic variational approach [42].

The rest of this paper is organized as follows. We first give a detailed description to our phase-field model in the next section. Then we construct our variational Lagrangian scheme by a discrete energetic variational approach in section 3. Plentiful numerical tests to validate our method are shown in section 4.

2. Model development. In this section, we give a detailed description of our phase-field model by an energetic variational approach [40, 34], including the motivation of proposing the energy-dissipation law (1.1).

2.1. Energetic variational approach. An energetic variational approach, originated from pioneering work of Onsager [48, 49] and Rayleigh [57], provides a general framework to determine the dynamics of a system from a prescribed energy-dissipation law through two distinct variational processes: the least action principle (LAP) and the maximum dissipation principle (MDP) [40, 34]. During the last decade, this

approach has been successfully applied to build up many mathematical models in physics, chemistry, and biochemistry [30, 40, 59, 28, 34, 64].

For an isothermal closed system, an energy dissipation is given by

$$\frac{\mathrm{d}}{\mathrm{d}t}E^{\mathrm{total}}(t) = -2\mathcal{D}(t), \tag{2.1}$$

which is the consequence of the first and second laws of thermodynamics [34]. Here E^{total} is the total energy, which is the sum of the Helmholtz free energy $\mathcal{F}$ and the kinetic energy $\mathcal{K}$, and $2\mathcal{D}$ is the rate of energy dissipation. The LAP states that the equation of motion for a Hamiltonian system can be derived from the variation of the action functional $\mathcal{A}(\boldsymbol{x}) = \int_0^T \mathcal{K} - \mathcal{F}\mathrm{d}t$ with respect to the flow map $\boldsymbol{x}$ (the trajectory in Lagrangian coordinates) if applicable [4, 34], i.e.,

$$\delta\mathcal{A} = \int_0^T \int_{\Omega(t)} (f_{\mathrm{inertial}} - f_{\mathrm{conv}}) \cdot \delta\boldsymbol{x}\mathrm{d}\boldsymbol{x}\mathrm{d}t. \tag{2.2}$$

It gives a unique procedure to derive the conservative force for the system. On the other hand, for a dissipative system ($\mathcal{D} \geq 0$), the dissipative force can be obtained by minimizing the dissipation functional $\mathcal{D}$ with respect to the "rate" $\boldsymbol{x}_t$ in the regime of linear response [22], known as Onsager's MDP, i.e.,

$$\delta\mathcal{D} = \int_{\Omega(t)} f_{\mathrm{diss}} \cdot \delta\boldsymbol{x}_t \ \mathrm{d}\boldsymbol{x}. \tag{2.3}$$

Hence, the force balance condition ($f_{\mathrm{inertial}} = f_{\mathrm{conv}} + f_{\mathrm{diss}}$) results in

$$\frac{\delta\mathcal{D}}{\delta\boldsymbol{x}_t} = \frac{\delta\mathcal{A}}{\delta\boldsymbol{x}}, \tag{2.4}$$

which is the dynamics of the system. We refer the reader to [34] for more detailed descriptions of energetic variational approaches and we only consider systems without the kinetic energy, i.e., $\mathcal{K} = 0$, throughout this paper.

2.2. Energetic variational approaches to phase-field models. From an energetic variational viewpoint, Allen–Cahn and Cahn–Hilliard type models provide a dynamics to minimize the free energy functional

$$\mathcal{F}[\varphi, \nabla\varphi] = \int_\Omega W(\varphi, \nabla\varphi)\mathrm{d}\boldsymbol{x} \tag{2.5}$$

for φ in some admissible set $\mathcal{H}$ subject to some boundary conditions on $\partial\Omega$. Here,

$$\varphi = \begin{cases} 1 & \text{Phase 1,} \\ -1 & \text{Phase 2,} \end{cases} \tag{2.6}$$

is a "phase" function introduced to identify two phases; $W(\varphi, \nabla\varphi)$ is the free energy density given by

$$W(\varphi, \nabla\varphi) = \frac{1}{2}|\nabla\varphi|^2 + V(\varphi), \tag{2.7}$$

where $V(\varphi)$ is the interfacial (potential) energy that is often taken as a double-well potential

$$V(\varphi) = \frac{1}{4\epsilon^2}(\varphi^2 - 1)^2. \tag{2.8}$$

Different phase-field models can be derived by different choices of admissible sets $\mathcal{H}$ and dissipation functionals $2\mathcal{D}$.

In Allen–Cahn type models, $\mathcal{H}$ is often chosen to be $H^1(\Omega)$ with a suitable boundary condition, and the energy-dissipation law is given by

$$\frac{\mathrm{d}}{\mathrm{d}t}\mathcal{F}(\varphi, \nabla\varphi) = -\int_\Omega \frac{1}{\gamma}|\varphi_t|^2 \mathrm{d}\boldsymbol{x}, \tag{2.9}$$

where $\gamma > 0$ is the dissipation rate [34]. We take $\gamma = 1$ in the following. The energy-dissipation law (2.9) can be viewed as a gradient flow of the phase function $\varphi(\boldsymbol{x}, t)$, which specifies the dynamics approaching equilibria of the system. According to the general framework of an energetic variational approach, the corresponding gradient flow equation can be derived by first performing the LAP with respect to φ and the MDP with respect to φ_t:

$$\begin{aligned} &\text{LAP}: \frac{\delta \mathcal{A}}{\delta \varphi} = -\frac{\delta \mathcal{F}}{\delta \varphi} = \nabla \cdot \frac{\partial W}{\partial \nabla \varphi} - \frac{\partial W}{\partial \varphi}, \\ &\text{MDP}: \frac{\delta \mathcal{D}}{\delta \varphi_t} = \varphi_t, \end{aligned} \tag{2.10}$$

where we assume all boundary terms vanish due to the given boundary condition. Then the force balance equation (2.4) leads to an Allen–Cahn type equation

$$\varphi_t = \nabla \cdot \frac{\partial W}{\partial \nabla \varphi} - \frac{\partial W}{\partial \varphi}. \tag{2.11}$$

A stationary solution of the Allen–Cahn type equation satisfies the Euler–Lagrangian equation of the functional (2.5), i.e.,

$$\frac{\delta W}{\delta \varphi} - \nabla \cdot \left(\frac{\delta W}{\delta \nabla \varphi} \right) = 0. \tag{2.12}$$

The above derivation performs an energetic variational approach in terms of φ and φ_t. We call this as the *Eulerian approach*, in which φ can be viewed as generalized coordinates of the system [24]. There is an alternative way to derive a dynamics of the system, known as the *Lagrangian approach* [34]. Instead of studying the evolution of phase function $\varphi(\boldsymbol{x}, t)$ directly, the Lagrangian approach studies the evolution of a *Lagrangian map*, or *flow map*, $\boldsymbol{x}(\mathbf{X}, t)$ for a given initial condition $\varphi_0(\mathbf{X})$. For fixed t, $\boldsymbol{x}^t(\mathbf{X}) = \boldsymbol{x}(\mathbf{X}, t)$ is a diffeomorphism between the initial domain Ω^0 and the current domain Ω^t, known as a *deformation map* [61, 35]. For fixed $\mathbf{X}$, $\boldsymbol{x}(\mathbf{X}, t)$ is the trajectory of the particle labeled by $\mathbf{X}$. We can view $\mathbf{X} \in \Omega^0$ as Lagrangian coordinates and $\boldsymbol{x} \in \Omega^t$ as Eulerian coordinates.

For a given flow map $\boldsymbol{x}(\mathbf{X}, t)$, we can define the virtual velocity in Eulerian coordinates $\mathbf{u}(\boldsymbol{x}(\mathbf{X}, t), t)$ as

$$\mathbf{u}(\boldsymbol{x}(\mathbf{X}, t), t) = \boldsymbol{x}_t(\mathbf{X}, t). \tag{2.13}$$

Another important quantity associated with $\boldsymbol{x}(\mathbf{X}, t)$ is the deformation tensor $F(\mathbf{X}, t)$, defined by

$$F(\mathbf{X}, t) = \nabla_{\mathbf{X}} \boldsymbol{x}(\mathbf{X}, t), \tag{2.14}$$

which carries all the information about how the physical quantity φ transports with the flow. Since $\boldsymbol{x}(\mathbf{X}, t)$ is a one-to-one map between Ω^0 and Ω^t for fixed t, we can enforce $\det F(\mathbf{X}, t) > 0$, which means the map $\boldsymbol{x}(\mathbf{X}, t)$ is orientation-preserving $\forall t$ [35].

In order to get the equation of $\boldsymbol{x}(\mathbf{X},t)$, we shall impose the kinematic relation to the physical quantity φ. Then the dynamics of $\varphi(\boldsymbol{x}(\mathbf{X},t),t)$ will be totally determined by the dynamics of the flow map $\boldsymbol{x}(\mathbf{X},t)$. For Allen–Cahn type models, it is often assumed that φ satisfies

$$\varphi(\boldsymbol{x}(\mathbf{X},t),t)=\varphi_0(\mathbf{X}), \tag{2.15}$$

where $\varphi_0(\mathbf{X})$ is the initial condition. One can view (2.15) as a composition between φ_0 and the inverse flow map $\mathbf{X}^{-1}(\boldsymbol{x},t)$ at time t, that is,

$$\varphi(\boldsymbol{x},t)=\varphi_0\circ\mathbf{X}^{-1}(\boldsymbol{x},t). \tag{2.16}$$

From the kinematic equation (2.15), we have

$$0=\frac{\mathrm{d}}{\mathrm{d}t}\varphi(\boldsymbol{x}(\mathbf{X},t),t)=\partial_t\varphi+\nabla\varphi\cdot\mathbf{u}. \tag{2.17}$$

Hence, $\varphi(\boldsymbol{x},t)$ satisfies the scalar transport equation

$$\partial_t\varphi+\mathbf{u}\cdot\nabla\varphi=0 \tag{2.18}$$

in Eulerian coordinates.

Remark 2.1. The above transport relation (2.18) is the macroscopic transport of the microscopic variable φ, which might only be valid locally. A complicated phase evolution, such as interface merging or pinching off, which is a consequence of microscopic evolution of φ, cannot be described by this kinematics.

Within the kinematics (2.15), $\varphi(\boldsymbol{x})$ is determined by $\boldsymbol{x}(\mathbf{X},t)$ for a given $\varphi_0(\mathbf{X})$. Hence, we can propose an energy-dissipation law in terms of $\boldsymbol{x}(\mathbf{X},t)$ and $\boldsymbol{x}_t(\mathbf{X},t)$ to characterize the dynamics of the flow map, that is,

$$\frac{\mathrm{d}}{\mathrm{d}t}\mathcal{F}[\boldsymbol{x}]=-2\mathcal{D}[\boldsymbol{x},\boldsymbol{x}_t], \tag{2.19}$$

where

$$\mathcal{F}[\boldsymbol{x}]=\int_{\Omega_0}W(\varphi_0,F^{-\mathrm{T}}\nabla_{\mathbf{X}}\varphi_0)\det F\mathrm{d}\mathbf{X}, \tag{2.20}$$

and $2\mathcal{D}[\boldsymbol{x},\boldsymbol{x}_t]\geq 0$ is the rate of energy dissipation. One can view the free energy as a functional of $\mathbf{X}$, $\boldsymbol{x}(\mathbf{X},t)$ and F, denoted by

$$\mathcal{F}[\boldsymbol{x}]=\int_{\Omega_0}\mathcal{W}(\mathbf{X},F)\mathrm{d}\mathbf{X}. \tag{2.21}$$

The energy-dissipation law (2.19) can be viewed as a generalized gradient flow of the flow map $\boldsymbol{x}(\mathbf{X},t)$. Since we are only concerned with equilibria of the system, the choice of dissipation only effects the dynamics approaching to equilibria. We'll discuss this later.

The evolution equation of the flow map $\boldsymbol{x}(\mathbf{X},t)$ can be derived by employing an energetic variational approach, that is,

$$\frac{\delta\mathcal{D}}{\delta\boldsymbol{x}_t}=-\frac{\delta\mathcal{F}}{\delta\boldsymbol{x}}, \tag{2.22}$$

where (see Appendix A for the detailed computation)

$$\frac{\delta \mathcal{F}}{\delta \boldsymbol{x}} = \nabla \cdot \left(\frac{\partial W}{\partial \nabla \varphi} \otimes \nabla \varphi - W(\varphi, \nabla \varphi) \mathrm{I} \right). \tag{2.23}$$

A stationary solution in the Lagrangian approach satisfies

$$\nabla \cdot \left(\frac{\partial W}{\partial \nabla \varphi} \otimes \nabla \varphi - W(\varphi, \nabla \varphi) \mathrm{I} \right) = 0. \tag{2.24}$$

Remark 2.2. The Lagrangian approach minimizes the free energy functional in the admissible set

$$\mathcal{Q} = \{ \varphi(\boldsymbol{x}) \mid \varphi(\boldsymbol{x}) = \varphi_0 \circ \mathbf{X}^{-1}(\boldsymbol{x}),\ \mathbf{X}^{-1} : \Omega \to \Omega^0 \}, \tag{2.25}$$

which is different from that in the Eulerian approach. So it is subtle to choose a suitable φ_0 to get a desired equilibrium. For the classical Allen–Cahn equation, since $|\varphi| \leq 1$, it is not difficult to choose a proper φ_0. In general, φ_0 can be obtained by some Eulerian solver. We can also update φ_0 during the evolution of the flow map.

Remark 2.3. If φ is a conserved quantity that satisfies

$$\frac{\mathrm{d}}{\mathrm{d}t} \int_\Omega \varphi(\boldsymbol{x}, t) \mathrm{d}\boldsymbol{x} = 0, \tag{2.26}$$

then the kinematic equation is given by

$$\varphi(\boldsymbol{x}(\mathbf{X}, t), t) = \frac{\varphi_0(\mathbf{X})}{\det F}. \tag{2.27}$$

This is the kinematics for the Cahn–Hilliard type equation, which can be viewed as a generalized diffusion with the energy-dissipation law given by [43]

$$\frac{\mathrm{d}}{\mathrm{d}t} \int_\Omega W(\varphi, \nabla \varphi) \mathrm{d}\boldsymbol{x} = - \int_\Omega \varphi^2 |\mathbf{u}|^2 \mathrm{d}\boldsymbol{x}. \tag{2.28}$$

Both Allen–Cahn and Cahn–Hilliard equations are driven by the same mixture energy (2.5), but the kinematics and dissipation mechanisms are different.

Although the equations for stationary solutions obtained by the Eulerian approach (variation on the phase variable $\varphi(\boldsymbol{x}, t)$) and the Lagrangian approach (variation on the flow map) look different ((2.12) and (2.24)), formally one can easily show as follows [41].

THEOREM 2.1. *For a given energy functional* (2.5)*, all smooth (regular enough) solutions of the Euler–Lagrangian equation*

$$-\nabla \cdot \left(\frac{\partial W}{\partial \nabla \varphi} \right) + \frac{\partial W}{\partial \varphi} = 0 \tag{2.29}$$

also satisfy the equation

$$\nabla \cdot \left(\frac{\partial W}{\partial \nabla \varphi} \otimes \nabla \varphi - W \mathrm{I} \right) = 0. \tag{2.30}$$

This result indicates connection between the variation with respect to φ and the variation with respect to the flow map through Legendre transform [41]. In general, the weak solution of the Euler–Lagrange equation (2.29) may not satisfy (2.30). In the theory of harmonic maps, a weak solution of (2.29) that also satisfies the weak form of (2.30) is known as a *stationary weak solution* [41, 53, 6]. From a numerical perspective, this theorem indicates that all equilibria in the Eulerian approach can be obtained from the Lagrangian approach with a proper choice $\varphi_0(\mathbf{X})$. However, for a given $\varphi_0(\mathbf{X})$, the Lagrangian calculation may not end up with the same equilibrium of the Eulerian approach.

2.3. Dissipation functional. In this subsection, we discuss the choice of dissipation functionals in Lagrangian approaches to phase-field models. Different choices of dissipations provide different dynamics approaching equilibria of the system. Since we may have multiple equilibria for the free energy like (2.5) [70], different dynamics may end up with different equilibria for the same $\varphi_0(\mathbf{X})$.

By using the kinematic relation (2.16) and (2.18), the dissipation in the gradient flow (2.9) can be reformulated in terms of $\boldsymbol{x}(\mathbf{X},t)$ and $\boldsymbol{x}_t(\mathbf{X},t)$, that is,

$$\mathcal{D}[\boldsymbol{x},\boldsymbol{x}_t] = -\frac{1}{2}\int |\nabla\varphi\cdot\mathbf{u}|^2 \mathrm{d}\boldsymbol{x} \tag{2.31}$$

for a given initial condition $\varphi_0(\mathbf{X})$. The equation of the flow map $\boldsymbol{x}(\mathbf{X},t)$ can be obtained via a standard energetic variational approach (2.22), which is

$$(\nabla\varphi\otimes\nabla\varphi)\mathbf{u} = -\nabla\cdot\left(\frac{\partial W}{\partial\nabla\varphi}\otimes\nabla\varphi - W(\varphi,\nabla\varphi)\mathrm{I}\right). \tag{2.32}$$

Here the right-hand side is obtained by the LAP, which corresponds to $\frac{\delta\mathcal{A}}{\delta\boldsymbol{x}}$ (see (2.23)), while the left-hand side is obtained by the MDP, i.e., $\frac{\delta\mathcal{D}}{\delta\mathbf{u}} = (\nabla\varphi\otimes\nabla\varphi)\mathbf{u}$. In a recent work [17], the authors studied numerical methods for equation (2.32) in one dimension by discretizing $\boldsymbol{x}(\mathbf{X},t)$ directly. Their results show that the dynamics (2.32) can capture the thin diffuse interfaces of Allen–Cahn type equations with a small number of mesh points in one dimension. However, the energy-dissipation law (2.31) may not be suitable for Lagrangian calculations, especially for high dimensions $d \geq 2$. Indeed, since $\nabla\varphi\otimes\nabla\varphi$ is a rank one matrix, $\nabla\varphi\otimes\nabla\varphi$ is not an invertible matrix for $d \geq 2$, so $\mathbf{u}$ is not well-defined everywhere. Moreover, even for one-dimensional (1D) cases, $\nabla\varphi\otimes\nabla\varphi$ is almost zero in noninterfacial regions, which restricts the choice of φ_0.

The degeneracy of (2.32) motivates us to consider a different dissipation functional by adding a new term, that is,

$$\mathcal{D} = \frac{1}{2}\int_\Omega |\nabla\varphi\cdot\mathbf{u}|^2 + \nu|\nabla\mathbf{u}|^2 \mathrm{d}\boldsymbol{x}, \tag{2.33}$$

where ν is a constant. By a direct computation, for such an energy-dissipation law, the dynamics of the system is given by

$$-\nu\Delta\mathbf{u} + (\nabla\varphi\otimes\nabla\varphi)\,\mathbf{u} = -\nabla\cdot\left(\frac{\partial W}{\partial\nabla\varphi}\otimes\nabla\varphi - W(\varphi,\nabla\varphi)\mathrm{I}\right), \tag{2.34}$$

which gives us the equation of the flow map $\boldsymbol{x}(\mathbf{X},t)$ in Lagrangian coordinates. The energy-dissipation law (2.33) fixes the degeneracy of $\nabla\varphi\otimes\nabla\varphi$. Moreover, from a computational perspective, $\nu|\nabla\mathbf{u}|^2$ can be viewed as a regularization term to the flow map $\boldsymbol{x}(\mathbf{X},t)$, which controls the quality of the mesh generated by the flow map.

In Lagrangian coordinates, (2.33) can be written as

$$\mathcal{D}[\boldsymbol{x}, \boldsymbol{x}_t] = \frac{1}{2}\int_{\Omega^0} \left|(F^{-\mathrm{T}}\nabla_{\mathbf{X}}\varphi_0)\cdot \boldsymbol{x}_t\right|^2 + \nu|\nabla_{\mathbf{X}}\boldsymbol{x}_t F^{-1}|^2 \det F \mathrm{d}\mathbf{X}. \tag{2.35}$$

In order to simplify the numerical implementation, we replace $|\nabla_{\mathbf{X}}\boldsymbol{x}_t F^{-1}|^2$ by $|\nabla_{\mathbf{X}}\boldsymbol{x}_t|$ in the following. Then the equation for the flow map $\boldsymbol{x}(\mathbf{X}, t)$ is given by (recall $\frac{\partial W}{\partial \nabla\varphi} = \nabla\varphi$ due to (2.7))

$$\begin{aligned} &-\nu\Delta_{\mathbf{X}}\mathbf{u} + \left((F^{-\mathrm{T}}\nabla_{\mathbf{X}}\varphi_0)\otimes(F^{-\mathrm{T}}\nabla_{\mathbf{X}}\varphi_0)\right)\mathbf{u} \\ &\quad = -\nabla_{\mathbf{X}}\left((F^{-\mathrm{T}}\nabla_{\mathbf{X}}\varphi_0)\otimes(F^{-\mathrm{T}}\nabla_{\mathbf{X}}\varphi_0) - W(\varphi_0, F^{-\mathrm{T}}\nabla_{\mathbf{X}}\varphi_0)\mathrm{I}\right) : F^{-1}, \end{aligned} \tag{2.36}$$

subject to the initial condition $\boldsymbol{x}(\mathbf{X}, 0) = \mathbf{X}$ and a suitable boundary condition, where $A : B = \sum_{j,k=1}^{n} A_{ijk}B_{jk}$ for $A \in \mathbb{R}^{n\times n\times n}$ and $B \in \mathbb{R}^{n\times n}$.

Remark 2.4. It is worth mentioning that the additional terms in both (2.33) and (2.35) are not physically acceptable viscosity for compressible fluids, and we add them into the dissipation functional only for numerical purposes. More specifically, let

$$\boldsymbol{x}^*(\mathbf{X}, t) = R(t)\boldsymbol{x}(\mathbf{X}, t); \tag{2.37}$$

then according to the frame-indifference, we should have

$$\mathcal{D}(\boldsymbol{x}, \boldsymbol{x}_t) = \mathcal{D}(\boldsymbol{x}^*, \boldsymbol{x}_t^*). \tag{2.38}$$

Note

$$\nabla_{\boldsymbol{x}^*}\mathbf{u}^* = \dot{R}R^{-1} + R\nabla_{\boldsymbol{x}}\mathbf{u}R^{-1}, \quad \nabla_{\mathbf{X}}\mathbf{u}^* = \dot{R}F + R\nabla_{\mathbf{X}}\mathbf{u},$$

hence, it is easy to show that the additional terms in both (2.33) and (2.35) conflict with the frame-indifference. For compressible flows, a physically acceptable viscosity in the dissipation is often taken as

$$\mathcal{D} = \int \nu\left|\frac{1}{2}(\nabla\mathbf{u} + (\nabla\mathbf{u})^{\mathrm{T}})\right|^2 + \left(\zeta - \frac{2}{3}\nu\right)|\nabla\cdot\mathbf{u}|^2 \mathrm{d}\boldsymbol{x}, \tag{2.39}$$

where $\nu > 0$ and $\eta > 0$. We refer the reader to [3, 21] for more detailed discussions.

At the end of this section, we should emphasize that the above derivation is rather formal, in which we assume that the flow map exists at least locally. The goal of this paper is to design some Lagrangian schemes that preserve the above variational structures in a discrete level. More analysis is certainly needed to show the existence of the flow map. We refer the interested reader to [29, 20] for some theoretical results on some related but different systems.

3. Numerical scheme. In this section, we construct our variational Lagrangian scheme for the phase-field model with the energy-dissipation law (1.1) by a discrete energetic variational approach [42]. Instead of considering a particular weak form of the flow map equation (2.36), a discrete energetic variational approach, which performs an energetic variational approach at a semidiscrete level, derives a "semi-discrete equation" that inherits the variational structure from a discrete energy-dissipation law directly. By introducing a proper temporal discretization to the semi-discrete equation, we can construct an energy stable Lagrangian scheme to our phase-field model.

3.1. A discrete energetic variational approach. In general, for a system without the kinetic energy, a discrete energy-dissipation law can be written as

$$\frac{\mathrm{d}}{\mathrm{d}t}\mathcal{F}_h(\boldsymbol{\Xi}(t)) = -2\mathcal{D}_h(\boldsymbol{\Xi}(t), \boldsymbol{\Xi}'(t)), \tag{3.1}$$

where $\boldsymbol{\Xi}(t) \in \mathbb{R}^K$ is the "discrete" state variable, $\mathcal{F}_h(\boldsymbol{\Xi}(t))$ is the discrete free energy, and $2\mathcal{D}_h(\boldsymbol{\Xi}(t), \boldsymbol{\Xi}'(t))$ is the discrete dissipation. One can obtain a discrete energy-dissipation law (3.1) from the continuous energy-dissipation law by discretizing either the physical quantity $\varphi(\boldsymbol{x}, t)$ (Eulerian approaches) or the flow map $\boldsymbol{x}(\mathbf{X}, t)$ (Lagrangian approaches) in space.

Similar to an energetic variational approach in a continuous level, the governing equation of $\boldsymbol{\Xi}(t)$, a system of nonlinear ODEs, can be obtained from the force balance equation

$$\frac{\delta \mathcal{D}_h}{\delta \boldsymbol{\Xi}'}(\boldsymbol{\Xi}(t), \boldsymbol{\Xi}'(t)) = -\frac{\delta \mathcal{F}_h}{\delta \boldsymbol{\Xi}}(\boldsymbol{\Xi}(t)), \tag{3.2}$$

where the right-hand side comes by performing the LAP, taking variation of the discrete action functional $\mathcal{A}_h(\boldsymbol{\Xi}(t)) = \int_0^T -\mathcal{F}_h(\boldsymbol{\Xi}(t))\mathrm{d}t$ with respect to $\boldsymbol{\Xi}(t)$, while the left-hand side comes by performing the MDP, taking variation of the discrete dissipation functional $\mathcal{D}_h(\boldsymbol{\Xi}(t), \boldsymbol{\Xi}'(t))$ with respect to $\boldsymbol{\Xi}'(t)$.

A discrete energetic variational approach follows the strategy of *discrete-then-variation*, which has been a powerful tool to construct numerical schemes for complicated systems with variational structures [33, 18, 13, 14, 69, 42]. Compared with the traditional *variation-then-discrete* approach, the semidiscrete equation obtained by a discrete energetic variational approach can automatically inherit the variational structure from the continuous level. One may obtain the same semidiscrete equation through a variation-then-discrete approach by choosing a particular weak form for the PDE.

For our phase-field model, in order to get a discrete energy-dissipation law, we first introduce a piecewise linear approximation to the flow map $\boldsymbol{x}(\mathbf{X}, t)$, which can be constructed by a standard finite element method. In the following, we only discuss the 2D case; the procedure can be easily extended to other spatial dimensions. Let $\mathcal{T}_h$ be a triangulation of the domain Ω^0, consisting of a set of simplexes $\{\tau_e \mid e = 1, \dots M\}$ and a set of nodal points $\mathcal{N}_h = \{\mathbf{X}_1, \mathbf{X}_2, \dots, \mathbf{X}_N\}$. Then the approximated flow map is given by

$$\boldsymbol{x}_h(\mathbf{X}, t) = \sum_{i=1}^{N} \boldsymbol{\xi}_i(t)\psi_i(\mathbf{X}) \ \in \ V_h, \tag{3.3}$$

where

$$V_h = \{v \in C(\Omega) \mid v \text{ is linear on each element } \tau_e \in \mathcal{T}_h\},$$

and $\psi_i(\mathbf{X}) : \mathbb{R}^2 \to \mathbb{R}$ is the hat function satisfying $\psi_i(\mathbf{X}_j) = \delta_{ij}$. Since $\boldsymbol{x}_h(\mathbf{X}_i, t) = \boldsymbol{\xi}_i(t)$, $\boldsymbol{\xi}_i(t) = (\xi_{i,x}, \xi_{i,y}) \in \mathbb{R}^2$ can be viewed as the coordinate of the ith mesh point at Ω^t, and $\boldsymbol{\xi}_i'(t)$ defines the velocity of ith mesh point. Within the above spatial discretization, the discrete state variable of the system $\boldsymbol{\Xi}(t)$ is defined by

$$\boldsymbol{\Xi}(t) = (\xi_{1,x}, \xi_{2,x}, \dots, \xi_{N,x}, \xi_{1,y}, \xi_{2,y}, \dots, \xi_{N,y}) \in \mathbb{R}^K, \tag{3.4}$$

where $K = 2N$. For simplicity's sake, we consider the natural boundary condition for the flow map through this section. For the Dirichlet boundary condition considered in the next section, if φ_0 is chosen to satisfy the Dirichlet boundary condition, we can set $x(\mathbf{X}, t) = \mathbf{X}$ for $\mathbf{X} \in \partial\Omega_0$, i.e., the velocity of the mesh points on the boundary to be zero, such that the Dirichlet boundary condition is satisfied for $\varphi(\boldsymbol{x}, t)$.

The framework of the finite element discretization enables us to compute the deformation matrix F explicitly on each element (see the appendix in [42] for the explicit form). We denote the deformation matrix $F_h(\boldsymbol{x}_h(\mathbf{X}, t), t)$ on each element τ_e, which is a constant matrix for fixed t, by $F_e(\boldsymbol{\Xi}(t)) = \nabla_{\mathbf{X}}|_{\mathbf{X}\in\tau_e}\boldsymbol{x}_h$. The admissible set of $\boldsymbol{\Xi}(t)$ is defined by

$$\mathcal{S}_{ad}^h = \left\{\boldsymbol{\Xi}(t) \in \mathbb{R}^K \mid \det F_e(\boldsymbol{\Xi}(t)) > 0 \ \ \forall e\right\}. \tag{3.5}$$

It can be noticed that $\mathcal{S}_{ad}^h$ is not a convex set, which imposes difficulties in both simulations and numerical analysis.

Inserting (3.3) into the original energy-dissipation law, we can obtain the discrete free energy

$$\mathcal{F}_h(\boldsymbol{\Xi}(t)) = \sum_{e=1}^{M} \int_{\tau_e} W\left(\varphi_0(X), F_e^{-\mathrm{T}}\nabla_X\varphi_0\right) \det F_e \mathrm{d}X \tag{3.6}$$

and the discrete dissipation functional

$$\mathcal{D}(\boldsymbol{\Xi}(t), \boldsymbol{\Xi}'(t)) = \frac{1}{2}\sum_{e=1}^{M} \int_{\tau_e} \left(|(F_e^{-\mathrm{T}}\nabla_{\mathbf{X}}\varphi_0)\cdot\mathbf{u}_h|^2 + \nu|\nabla_{\mathbf{X}}\mathbf{u}_h|^2\right) \det F_e \mathrm{d}\mathbf{X}, \tag{3.7}$$

where

$$\mathbf{u}_h(\mathbf{X}, t) = \sum_{j=1}^{N} \boldsymbol{\xi}_j'(t)\psi_j(\boldsymbol{X}). \tag{3.8}$$

Then by a discrete energetic variation approach, we can derive a system of ordinary differential equations of $\boldsymbol{\Xi}(t)$, that is,

$$\mathsf{D}_h(\boldsymbol{\Xi}(t))\boldsymbol{\Xi}'(t) = -\frac{\delta\mathcal{F}_h}{\delta\boldsymbol{\Xi}}(\boldsymbol{\Xi}(t)). \tag{3.9}$$

We refer readers to the appendix for the detailed computation of $\mathsf{D}(\boldsymbol{\Xi}(t))$ and the $\frac{\delta\mathcal{F}_h}{\delta\boldsymbol{\Xi}}$. Although the explicit forms of both $\mathsf{D}(\boldsymbol{\Xi}(t))$ and $\frac{\delta\mathcal{F}}{\delta\boldsymbol{\Xi}}$ may not be available in a general mesh, both of them are easy to obtain during the numerical implementation by summing the results on each element over the mesh. It can be noticed that $\mathsf{D}(\boldsymbol{\Xi}(t)) \in \mathbb{R}^{K\times K}$ given by

$$\mathsf{D}(\boldsymbol{\Xi}(t)) = \mathsf{M}(\boldsymbol{\Xi}(t)) + \nu\mathsf{K}(\boldsymbol{\Xi}(t)) \tag{3.10}$$

with

$$\mathsf{M} = \begin{pmatrix} \mathsf{M}_{xx} & \mathsf{M}_{xy} \\ \mathsf{M}_{yx} & \mathsf{M}_{yy} \end{pmatrix}, \quad \mathsf{K} = \begin{pmatrix} \mathsf{K}_0 & 0 \\ 0 & \mathsf{K}_0 \end{pmatrix}.$$

Here $\mathsf{M}_{\alpha\beta}$ $(\alpha, \beta = x, y)$ is the modified mass matrix defined by

$$\mathsf{M}_{\alpha\beta}(i, j) = \sum_{e\in N(i)} \partial_\alpha\varphi(\boldsymbol{x}_e)\partial_\beta\varphi(\boldsymbol{x}_e) \det F_e \int_{\tau_e} \psi_i\psi_j \mathrm{d}\mathbf{X}, \tag{3.11}$$

where $\boldsymbol{x}_e$ is the centroid of $\boldsymbol{x}^t(\tau_e)$, and K_0 is the modified stiff matrix defined by

$$\mathsf{K}_0(i,j) = \sum_{e\in N(i)} \det F_e \int_{\tau_e} \nabla_{\mathbf{X}}\psi_i \cdot \nabla_{\mathbf{X}}\psi_j \mathrm{d}\mathbf{X}. \tag{3.12}$$

It is easy to show that $\det \mathsf{M}(\boldsymbol{\Xi}) = 0$, M is positive semidefinite, and $\mathsf{K}(\boldsymbol{\Xi})$ is a positive-definite matrix if $\boldsymbol{\Xi} \in \mathcal{S}_{ad}^h$ (see Appendix B). Hence, the presence of $\nu\mathsf{K}$ ensures that D is positive definite.

3.2. Temporal discretization. Now we discuss the temporal discretization. A numerical scheme can be obtained by introducing a suitable temporal discretization to the semidiscrete equation (3.9). An advantage of a variational structure in the semidiscrete level is that various classical numerical schemes can be reformulated as optimization problems [26, 68, 46]. In the current study, we use the implicit Euler for temporal discretization. It is not difficult to apply high-order temporal discretization, such as the BDF2 or the Crank–Nicolson [26] to our system, which will be studied in future work.

For given $\boldsymbol{\Xi}^n \in \mathcal{S}_{ad}^h$, the implicit Euler scheme for (3.9) is given by

$$\mathsf{D}_*^n \frac{\boldsymbol{\Xi}^{n+1} - \boldsymbol{\Xi}^n}{\tau} = -\frac{\delta \mathcal{F}_h}{\delta \boldsymbol{\Xi}}(\boldsymbol{\Xi}^{n+1}), \tag{3.13}$$

where D_*^n is chosen to be independent with $\boldsymbol{\Xi}^{n+1}$, that is, taking $\partial_\alpha\varphi$, $\partial_\beta\varphi$, and $\det F_e$ in (3.11) and (3.12) to be their values at the nth step.

Although (3.13) is a system of highly nonlinear equations that is often difficult to solve, by virtue of the variational structures in the semidiscrete level, we can reformulate (3.13) into an optimization problem, given by

$$\boldsymbol{\Xi} = \mathrm{argmin}_{\boldsymbol{\Xi}\in\mathcal{S}_{ad}^h} J_n(\boldsymbol{\Xi}), \tag{3.14}$$

where

$$J_n(\boldsymbol{\Xi}) = \frac{(\mathsf{D}_*^n(\boldsymbol{\Xi} - \boldsymbol{\Xi}^n), (\boldsymbol{\Xi} - \boldsymbol{\Xi}^n))}{2\tau} + \mathcal{F}_h(\boldsymbol{\Xi}). \tag{3.15}$$

There are various advantages in solving optimization problem (3.14) instead of solving the original nonlinear system (3.13) directly. Since $J_n(\boldsymbol{\Xi})$ might not be a convex function, solving (3.13) with standard nonlinear solvers, such as fixed-point iterations or Newton type methods, may only obtain a saddle point or a local minimizer of $J_n(\boldsymbol{\Xi})$, which may not decrease the discrete energy. Moreover, the standard nonlinear solver cannot guarantee that the obtained solution is in the admissible set $\mathcal{S}_{ad}^h$. For the optimization problem (3.14), we can use some line-search-based optimization method and manually set

$$J_n(\boldsymbol{\Xi}) = \infty, \quad \boldsymbol{\Xi} \notin \mathcal{S}_{ad}^h.$$

Then the line-search-based method can guarantee $\det F_e > 0$ as if $J_n(\boldsymbol{\Xi}^{n+1}) \le J_n(\boldsymbol{\Xi}^n)$, even though the exact global minimizer of $J_n(\boldsymbol{\Xi})$ may not be found. Noticed that $J(\boldsymbol{\Xi}^{n+1}) \le J(\boldsymbol{\Xi}^n)$ indicates

$$\frac{1}{2\tau}\mathsf{D}_n^*(\boldsymbol{\Xi}^{n+1} - \boldsymbol{\Xi}^{\boldsymbol{n}}) \cdot (\boldsymbol{\Xi}^{n+1} - \boldsymbol{\Xi}^{\boldsymbol{n}}) + \mathcal{F}_h(\boldsymbol{\Xi}^{n+1}) \le \mathcal{F}_h(\boldsymbol{\Xi}^n). \tag{3.16}$$

Hence, our scheme is energy stable and satisfies the discrete energy-dissipation law

$$\frac{\mathcal{F}_h(\boldsymbol{\Xi}^{n+1}) - \mathcal{F}_h(\boldsymbol{\Xi}^n)}{\tau} \le -\frac{1}{2\tau^2}\mathsf{D}_n^*(\boldsymbol{\Xi}^n - \boldsymbol{\Xi}^{n+1}) \cdot (\boldsymbol{\Xi}^n - \boldsymbol{\Xi}^{n+1}) \le 0. \tag{3.17}$$

Under suitable conditions, following [11], we can prove the existence of a minimal solution of the optimization problem (3.14).

PROPOSITION 3.1. *For a given initial condition $\varphi_0(\mathbf{X})$, if the free energy density $\mathcal{W}(\mathbf{X}, F)$ (see (2.21) for the definition) satisfies $\mathcal{W}(\mathbf{X}, F) > 0$ for $\det F > 0$ and*

$$\mathcal{W}(\mathbf{X}, F) \to 0, \quad as \quad \det F \to \infty, \tag{3.18}$$

then for a given $\boldsymbol{\Xi}^n \in \mathcal{S}_{ad}^h$, there exists a solution $\boldsymbol{\Xi}^{n+1}$ to numerical scheme (3.13) such that the discrete energy-dissipation law (3.17) holds.

Proof. Due to the assumption (3.18), we know for $\forall \boldsymbol{\Xi} \in \partial \mathcal{S}_{ad}^{\boldsymbol{\Xi}}$, $J_n(\boldsymbol{\Xi}) = \infty$. Following the proof in Lemma 3.1 in [11], the existence of a minimizer can be obtained by showing the set

$$\mathcal{A} = \{\boldsymbol{\Xi} \in \mathcal{S}_{ad}^h \mid J_n(\boldsymbol{\Xi}) \le \mathcal{F}_h(\boldsymbol{\Xi}^n)\} \tag{3.19}$$

is a nonempty compact subset of $\mathbb{R}^K$. Obviously, $\boldsymbol{\Xi}^n \in \mathcal{A}$, so $\mathcal{A}$ is nonempty. On the other hand, since D_n^* is positive definite, there exists $\lambda_1 > 0$ such that $\forall \boldsymbol{\Xi} \in \mathcal{S}_{ad}^h$

$$\|\boldsymbol{\Xi} - \boldsymbol{\Xi}^n\|^2 \le \frac{1}{\lambda_1} \mathsf{D}_n^*(\boldsymbol{\Xi} - \boldsymbol{\Xi}^{\boldsymbol{n}}) \cdot (\boldsymbol{\Xi} - \boldsymbol{\Xi}^{\boldsymbol{n}}) \le \frac{2\tau}{\lambda_1} \left(\mathcal{F}_h(\boldsymbol{\Xi}^n) - \mathcal{F}_h(\boldsymbol{\Xi})\right), \tag{3.20}$$

which indicates $\mathcal{A}$ is bounded. So we only need to show $\mathcal{A}$ is closed in $\mathbb{R}^K$. For any converged sequence $\{\boldsymbol{\Xi}^{(k)}\}_{k=1}^{\infty} \subset \mathcal{S}_{ad}^h$, our goal is to show that the limit $\widetilde{\boldsymbol{\Xi}}$ is in $\mathcal{S}_{ad}^h$. Note for $\forall e \in \{1, 2, \dots M\}$ and $\forall k$,

$$\mathcal{F}_h(\boldsymbol{\Xi}^n) \ge \mathcal{F}_h(\boldsymbol{\Xi}^{(k)}) \ge \mathcal{W}(\mathbf{X}_e, F_e)|\tau_e|, \tag{3.21}$$

where $|\tau_e|$ is the area of element τ_e. Since $\mathcal{W}(X, F) \to \infty$ if $\det F \to 0$, we can conclude that $\det F_e(\boldsymbol{\Xi}^{(k)}) > 0$ is uniformly bounded away from zero. So $\det F_e(\widetilde{\boldsymbol{\Xi}}) > 0 \, \forall e$, which means $\widetilde{\boldsymbol{\Xi}} \in \mathcal{S}_{ad}^h$.

If $\boldsymbol{\Xi}^{n+1}$ is a global minimizer of $J_n(\boldsymbol{\Xi})$ in $\mathcal{S}_{ad}^h$, we have (3.16) and (3.17), which completes the proof. ∎

Under the same condition, we can prove the convergence of series $\{\boldsymbol{\Xi}^n\}$ for the discrete scheme for the given triangulation and fixed τ.

PROPOSITION 3.2. *For the given triangulation and fixed τ, if the free energy density $\mathcal{W}(\mathbf{X}, F)$ (see (2.21) for the definition) satisfies $\mathcal{W}(\mathbf{X}, F) > 0$ for $\det F > 0$ and*

$$\mathcal{W}(\mathbf{X}, F) \to 0, \quad \det F \to \infty, \tag{3.22}$$

for a given $\varphi_0(\mathbf{X})$, then the series $\{\boldsymbol{\Xi}^n\}$ converges to a stationary solution of the discrete energy $\mathcal{F}_h(\boldsymbol{\Xi})$.

Proof. We first prove that there exist c_0 such that

$$\boldsymbol{\Xi}^{\mathrm{T}} \mathsf{D}_n^* \boldsymbol{\Xi} \ge c_0 \|\boldsymbol{\Xi}\|^2 \quad \forall \boldsymbol{\Xi} \in \mathbb{R}^K.$$

Since M_n^* is nonnegative (see Appendix A for the proof), we only need to show, for $(\mathsf{K}_0)_{\mathsf{n}}^*$, that there exist c_0' such that

$$\boldsymbol{\alpha}^{\mathrm{T}} (\mathsf{K}_0)_n^* \boldsymbol{\alpha} \ge c_0' \|\boldsymbol{\alpha}\|^2 \quad \forall \boldsymbol{\alpha} \in \mathbb{R}^N.$$

Indeed, noting $\mathcal{F}_h(\boldsymbol{\Xi}^n) \le \mathcal{F}_h(\boldsymbol{\Xi}^0)$, we have

$$\mathcal{F}_h(\boldsymbol{\Xi}^0) \ge \mathcal{F}_h(\boldsymbol{\Xi}^n) \ge \mathcal{W}(\mathbf{X}_e, F_e)|\tau_e|,$$

and following the same argument in the proof of the previous proposition, we can show that $\det F_e$ is uniformly bounded away from zero, i.e., there exists $c_b > 0$ such that $\det F_e(\boldsymbol{\Xi}^n) > c_b \ \forall e$. Hence,

$$\boldsymbol{\alpha}^{\mathrm{T}}(\mathsf{K}_0)_n^*\boldsymbol{\alpha} = \sum_{e=1}^{M}\int_{\tau_e}\left|\sum_{i=1}^{N}\alpha_i\nabla\psi_i\right|^2 \det F_e \mathrm{d}\mathbf{X} \ge c_b\int_{\Omega}\left|\alpha_i\nabla\psi_i\right|^2\mathrm{d}\mathbf{X} \ge c_b\lambda_1\|\boldsymbol{\alpha}\|^2,$$

where $\lambda_1 > 0$ is the smallest eigenvalue of the stiff matrix.

Then by Proposition 3.1, we have

$$\begin{aligned} c_0\|\boldsymbol{\Xi}^{n+1} - \boldsymbol{\Xi}^n\|^2 &< \left(\mathsf{D}_*^n(\boldsymbol{\Xi}^{n+1} - \boldsymbol{\Xi}^n), \boldsymbol{\Xi}^{n+1} - \boldsymbol{\Xi}^n\right) \\ &\le 2\tau(\mathcal{F}_h(\boldsymbol{\Xi}^n) - \mathcal{F}_h(\boldsymbol{\Xi}^{n+1})). \end{aligned} \tag{3.23}$$

Hence,

$$\sum_{k=0}^{n} c_0\|\boldsymbol{\Xi}^{k+1} - \boldsymbol{\Xi}^k\|^2 \le 2\tau(\mathcal{F}_h(\boldsymbol{\Xi}^0) - \mathcal{F}_h(\boldsymbol{\Xi}^{n+1})) \le C, \tag{3.24}$$

where C is independent with n. So

$$\lim_{k\to\infty}\|\boldsymbol{\Xi}^{k+1} - \boldsymbol{\Xi}^k\|^2 = 0, \tag{3.25}$$

which indicates the series $\{\boldsymbol{\Xi}_k\}_{k=1}^{\infty}$ converges to some point in $\mathbb{R}^K$, denoted by $\boldsymbol{\Xi}^*$. Following the same argument in the proof of Proposition 3.1, we can show $\boldsymbol{\Xi}^* \in \mathcal{S}_{ad}^h$. Moreover, since

$$\lim_{n\to\infty}\frac{\delta\mathcal{F}_h}{\delta\boldsymbol{\Xi}}(\boldsymbol{\Xi}^{n+1}) = \lim_{n\to\infty} -\frac{1}{\tau}D_n^*(\boldsymbol{\Xi}^{n+1} - \boldsymbol{\Xi}^n), \tag{3.26}$$

we have $\frac{\delta\mathcal{F}_h}{\delta\boldsymbol{\Xi}}(\boldsymbol{\Xi}^*) = 0$, so $\boldsymbol{\Xi}^*$ is a stationary solution of the discrete energy $\mathcal{F}_h(\boldsymbol{\Xi})$. ∎

It should be emphasized that the condition (3.18) doesn't hold for the classical phase-field free energy. Hence, it might be difficult to show the existence of the solution to the numerical scheme that minimizes the $J_n(\boldsymbol{\Xi})$. Moreover, even if the minimizer of $J_n(\boldsymbol{\Xi})$ exists, our line-search-based optimization cannot guarantee to find it in each iteration. This is a limitation of the current numerical approach. In practice, we choose a small value of τ and a large value of ν such that the optimization problem can be handled by a standard optimization method, such as the L-BFSG. Indeed, the first term in (3.15) can be viewed as a regularization term, which restricts us to finding a minimizer around $\boldsymbol{\Xi}^n$. The positive definite condition on D_n^* is crucial; otherwise, $J_n(\boldsymbol{\Xi})$ may have infinite minimizers even around $\boldsymbol{\Xi}^n$. In all numerical experiments shown in the next section, we adopt the L-BFGS with a line search to find a minimizer $\boldsymbol{\Xi}^{n+1}$ in the admissible set that decreases the discrete energy. Lagrangian calculations will terminate if no $\boldsymbol{\Xi}^{n+1}$ is found or $|\mathcal{F}_h(\boldsymbol{\Xi}^{n+1}) - \mathcal{F}_h(\boldsymbol{\Xi}^n)| \le \epsilon$, where ϵ is the given tolerance.

3.3. Reinitialization. In the numerical implementation, we can compute $\boldsymbol{x}_h^{n+1}$ by

$$\boldsymbol{x}_h^{n+1}(\mathbf{X}) = \widetilde{\boldsymbol{x}}_h^{n+1} \circ \boldsymbol{x}_h^n(\mathbf{X}), \tag{3.27}$$

which is equivalent to setting $\mathbf{X}_i = \boldsymbol{\xi}_i^n$ after each iteration as in [39]. An advantage of this treatment is that in each iteration, we only need to compute a close to identity map [39]. So the optimization problem (3.14) is often easy to solve.

One can view this as a reinitialization procedure. A more complicated reinitialization procedure can be incorporated in our numerical framework. Indeed, for the given $\boldsymbol{x}^n(\mathbf{X})$, we also obtain a numerical solution φ^n defined at mesh points, that is,

$$\varphi^n(\boldsymbol{\xi}_i^n) = \varphi_0(\mathbf{X}). \tag{3.28}$$

When the mesh becomes too skewed, we can interpolate the numerical solution φ^n into a more regular mesh, obtained by coarsening or refining the current mesh [7]. More importantly, we can also apply an Eulerian solver by using φ^n as the initial condition, to update the value at each mesh point. This is close to the idea in the velocity-based moving mesh method [5], which updates both positions and values of mesh points. Unlike the traditional velocity-based moving mesh methods, our solution is spontaneously updated when the mesh moves. We'll explore reinitialization procedures in detail in future work.

4. Numerical validation and discussion. In this section, we apply our Lagrangian scheme to several problems modeled by Allen–Cahn type phase-field models. Most of the numerical examples used here were widely studied by Eulerian methods previously [16, 31, 56, 23, 72]. Numerical results show that, by choosing a suitable initial condition, our method can capture the thin diffuse interfaces with a small number of mesh points and reach a desired equilibrium.

Since we might need to apply a few Eulerian steps in the following numerical examples, here we briefly introduce the Eulerian method that we'll use. There are a lot of Eulerian methods for Allen–Cahn type phase-field models. In the spirit of the "discrete-then-variation" approach, here we use an Eulerian solver derived by the discrete energetic variational approach. We use the same finite element space with the Lagrangian solver and approximate the phase variable φ by

$$\varphi_h(X,t) = \sum_{i=1}^{N} \gamma_i(t)\psi_i(X), \tag{4.1}$$

where $\psi_i(X)$ are hat functions on the current mesh. Inserting (4.1) into the continuous energy-dissipation law, we can get a discrete energy-dissipation law with the discrete energy and the discrete dissipation given by

$$\begin{aligned} \mathcal{F}_h^{\text{Euler}} &= \sum_{e=1}^{N} \int_{\tau_e} \frac{1}{2} \left| \sum_{i=1}^{N} \gamma_i \nabla \psi_i(\mathbf{X}) \right|^2 + \frac{1}{4\epsilon^2} \sum_{i=1}^{N} (\gamma_i^2 - 1)^2 \psi_i(\mathbf{X}) \mathrm{d}\mathbf{X}, \\ \mathcal{D}_h^{\text{Euler}} &= \sum_{e=1}^{N} \int_{\tau_e} \left| \sum_{i=1}^{N} \gamma_i'(t) \psi_i(\mathbf{X}) \right|^2 \mathrm{d}\mathbf{X}, \end{aligned} \tag{4.2}$$

respectively, where we also introduce the piecewise linear approximation to the nonlinear term in the discrete energy. This form of the discrete energy was used in [68] and has an advantage in preserving the maximum principle at the discrete level [68]. After we obtain the semidiscrete equation of $\gamma_i(t)$, we solve it by the implicit Euler method, which can also be reformulated into a minimization problem, similar to (3.14). Indeed, the Eulerian solver we used here is similar to that in [68].

4.1. Quasi-1D example. First, we consider a quasi-1D problem, in which $\Omega = [-1,1]^2$. We impose a Dirichlet boundary condition on $x = -1$ and 1, that is,

$$\varphi(t,-1,y) = -1, \quad \varphi(t,1,y) = 1, \tag{4.3}$$

and a Neumann boundary condition on $y = -1$ and 1, that is,

$$\frac{\partial \varphi}{\partial y}(t,x,\pm 1) = 0. \tag{4.4}$$

If the initial condition $\varphi_0(\mathbf{X})$ satisfies (4.3) and (4.4), we can impose the boundary condition

$$\boldsymbol{x}(\pm 1, Y, t) = (\pm 1, Y), \quad \boldsymbol{x}(X, \pm 1, t) = (x, \pm 1) \tag{4.5}$$

for the flow map $\boldsymbol{x}(\mathbf{X},t) : (X,Y) \mapsto (x,y)$ such that $\varphi(\boldsymbol{x}(\mathbf{X},t))$ satisfies (4.3) and (4.4). The boundary condition (4.5) can be satisfied if $\mathbf{u}(X,Y)$ satisfies

$$\mathbf{u}(t,\pm 1,Y) = 0, \quad \mathbf{u}(t,X,\pm 1)\cdot \boldsymbol{n} = 0, \tag{4.6}$$

where $\boldsymbol{n} = (0,1)^{\mathrm{T}}$. In the following, we take the initial condition as

$$\varphi_0(X,Y) = -\tanh(5X). \tag{4.7}$$

Typical meshes and computed solutions for $\epsilon^2 = 10^{-4}$ and $\nu = 0.05$ at $t = 0, 0.01$ and 0.2 are shown Figure 4.1(a)–(c). The initial mesh is the uniform mesh with $M = 400$. We compare the obtained equilibrium solution with the 1D exact solution $\varphi(x) = -\tanh(\frac{x}{\sqrt{2}\epsilon})$ in Figure 4.1(d), in which the circles represent the projection of mesh points in the x-z plane, and the red line is the exact solution. It can be noticed that the equilibrium numerical solution can capture the thin interface with a small number of mesh points. Due to the presence of the $|\nabla \mathbf{u}|^2$ term in the dissipation, the vertical velocity of all mesh points is almost zero, which is essential for a successful Lagrangian computation in this case.

Figure 4.1(e) shows the discrete energy as a function of time t for different values of ν. One can notice that our scheme is energy stable in all cases and all calculations go to the same equilibrium. The convergence to the equilibrium becomes slower when ν becomes larger. On the other hand, numerical tests show that the optimization problem (3.14) in each iteration will be easier to solve for larger ν. In general, the value of ν also affects the quality of the obtained mesh. We are not going to discuss the choice of ν in this paper; in the following, we choose larger ν for smaller ϵ^2.

Compared with the Eulerian method, the Lagrangian method has an advantage in capturing the diffuse interface with a small number of number points. However, the numerical approximation in the bulk region might be poor since most of the mesh points are concentrated in the interface region. To illustrate this, we perform an accuracy test for this example. Since the solution is y-invariant, we take $\Omega = [-1,1] \times [-0.1, 0.1]$ in the accuracy test and only look at the numerical error for the equilibrium solution on $y = -0.1$ in the following. In Figure 4.2(a)–(b), we show the numerical error obtained by the Lagrangian (blue circles) at each mesh point on $y = -0.1$ with $h = 0.2$ and $h = 0.1$, respectively. It can be noticed that in both cases, the numerical error attains its maximum at the transition area between the diffuse interface and the bulk region. We can apply the Eulerian solver to the obtained solution; the numerical error after applying the Eulerian solver is shown in Figure 4.2

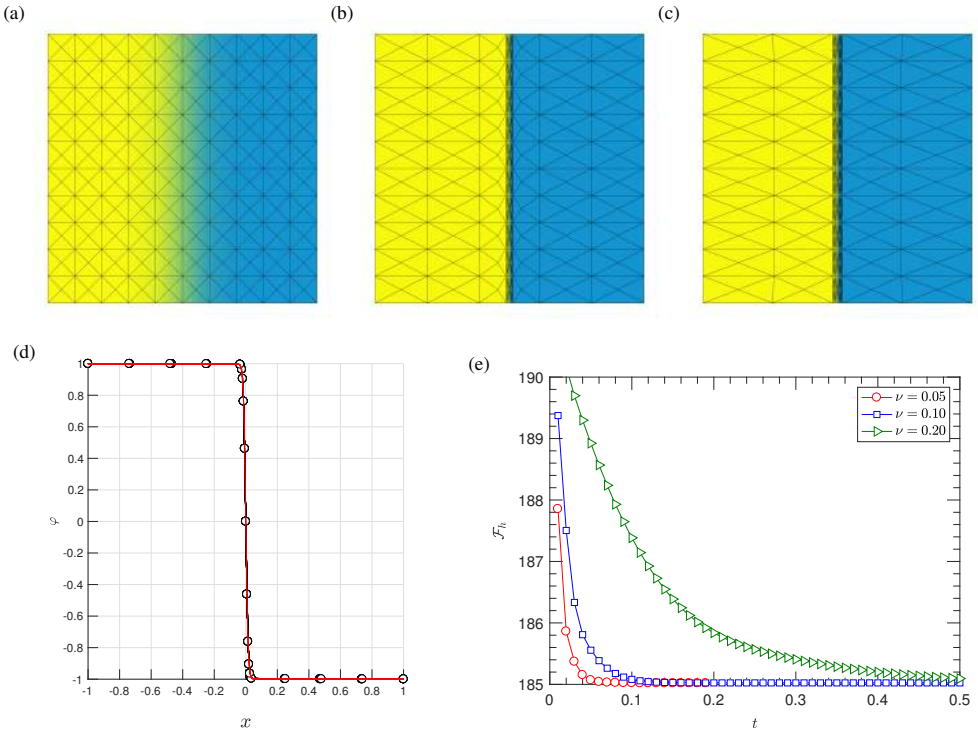

FIG. 4.1. *Numerical results for the quasi-1D example with* $\epsilon^2 = 1e-4$. (a)–(c) *Initial conditions and numerical solutions at* $t = 0.01$ *and* $t = 0.2$ *(equilibrium).* (d) *Side view of the equilibrium solution, compared with the* 1*D exact solution.* (e) *Discrete free energy* $\mathcal{F}_h$ *along with time for various* ν.

by red squares. Interestingly, although the Eulerian solver decreases the L^2-error of the numerical solution (so is the discrete free energy), the numerical error near the interface might increase a bit. This simple numerical test suggests that the Lagrangian method has an advantage in capturing the thin diffuse interface, while the Eulerian method can achieve better numerical approximation to the solution in the bulk region. We should emphasize that for the phase-field type model, Eulerian methods cannot obtain the right results if the mesh size is larger than the diffuse interface. So it is a natural idea to combine the Lagrangian method with some Eulerian method.

We quantify the numerical error for the Lagrangian method with different choices of h for $\epsilon^2 = 10^{-3}$ and 10^{-4}, shown in Table 4.1. The error in space is measured by the L^∞-norm defined by

$$\|e_h\|_\infty = \max_{i\in\{1,2,\dots N\}} |\varphi^h(\boldsymbol{x}_h(\mathbf{X}_i, T)) - \varphi^{eq}(\boldsymbol{x}_h(\mathbf{X}_i))|,$$

where T is the final time for Lagrangian calculations. Here we only test the convergence rate near the interface. It can be noticed that near the interface, our Lagrangian method can achieve second order accuracy in space. Another interesting phenomenon is that the numerical performance seems to be independent with ϵ. We should also mention that the numerical error also is sensitive to the choice of the initial condition $\varphi_0(\mathbf{X})$. A detailed numerical analysis is needed in order to understand these phenomena for the Lagrangian method.

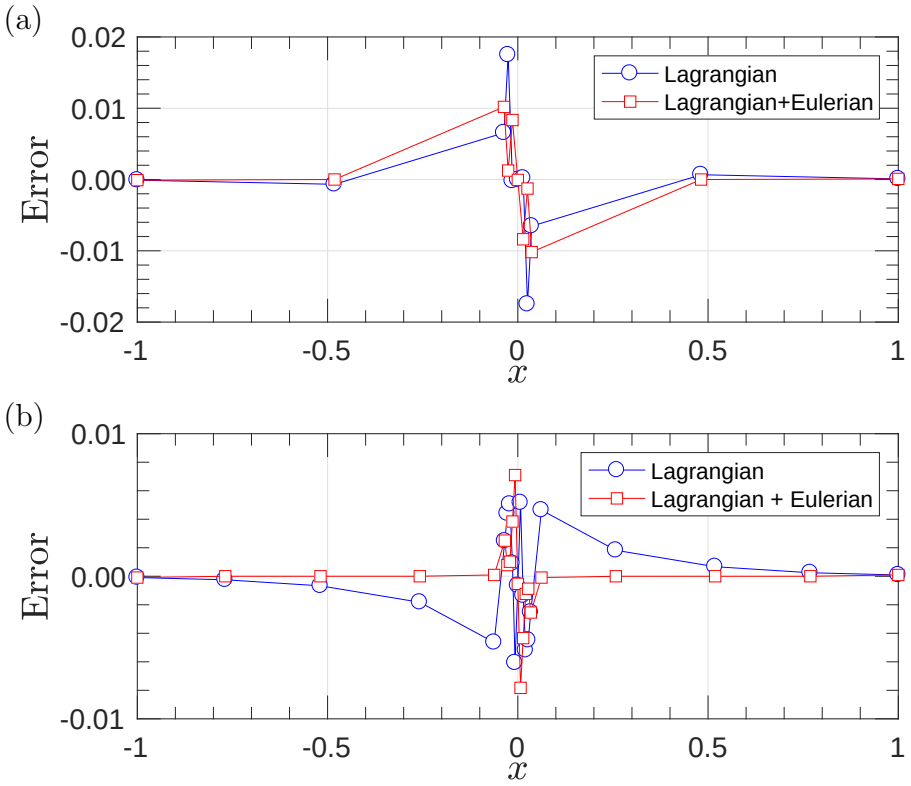

FIG. 4.2. *The numerical error on $y = -0.1$ for the equilibrium solution, obtained by Lagrangian and Lagrangian+Eulerian methods:* (a) $h = 0.2$ *and* (b) $h = 0.1$.

TABLE 4.1
The convergence rate of numerical solutions near the interface ($x \in [-3\epsilon, 3\epsilon]$) with $\nu = 0.05$.

$\epsilon^2 = 10^{-3}$				$\epsilon^2 = 10^{-4}$			
h	τ	L^∞-error	Order	h	τ	L^∞-error	Order
0.2	1/100	0.0185		0.2	1/100	0.0175	
0.1	1/400	0.0059	1.6487	0.1	1/400	0.0052	1.7508
0.05	1/1600	0.0015	1.9758	0.05	1/1600	0..0015	1.7935

4.2. Shrinkage of a circular domain. As a numerical test, we consider shrinkage of a circular domain in two dimensions. It is a classical benchmark problem for the Allen–Cahn equation [16, 31, 56], in which the circular interface governed by the Allen–Cahn equation will shrink and eventually disappear.

We take $\Omega = [-1, 1]^2$ and impose the Dirichlet condition $\varphi(\boldsymbol{x}) = -1, \boldsymbol{x} \in \partial\Omega$. The initial condition $\varphi_0(\mathbf{X})$ is taken as

$$\varphi_0(\mathbf{X}) = \tanh(10(\sqrt{X^2 + Y^2} - 0.5)), \tag{4.8}$$

such that the Dirichlet condition satisfies numerically. It is worth pointing out that for our Lagrangian method, it is crucial to choose a proper initial condition. For phase field models, $\varphi_0(\mathbf{X})$ is often chosen in a hyperbolic tangent form such that $\varphi_0 \in [-1, 1]$, and the width of the initial interface should be larger than the mesh size, since we need enough mesh points in the region of interfaces.

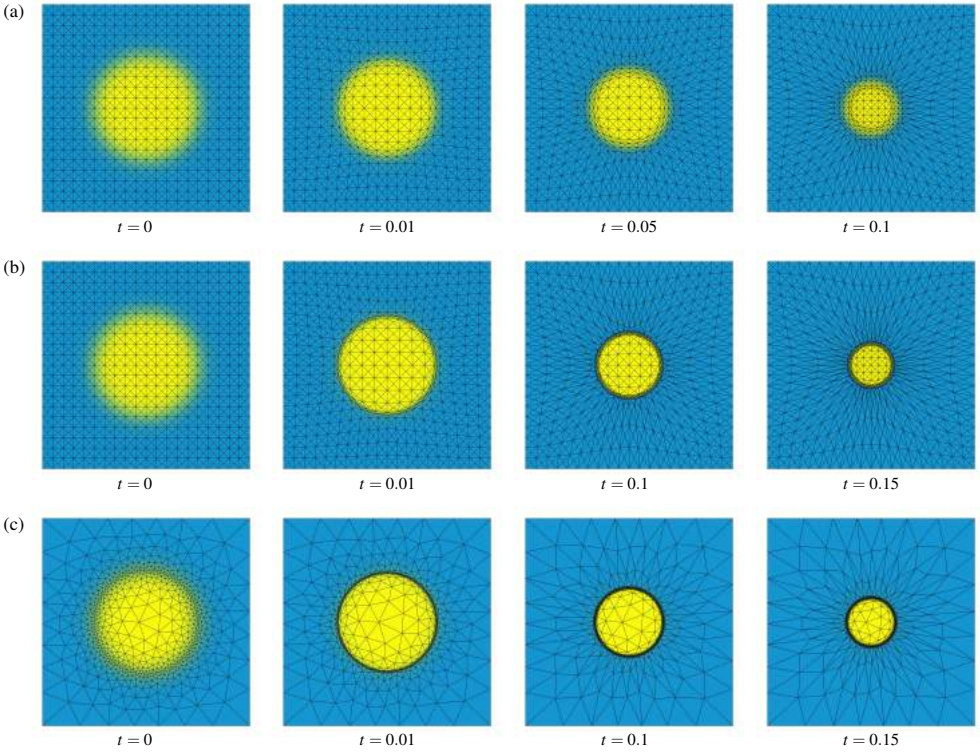

FIG. 4.3. (a) *Numerical results of the evolution of the circular domain for* $\epsilon^2 = 10^{-3}$ *[*$\tau = 10^{-2}$*].* (b)–(c) *Numerical results of the evolution of the circular domain for* $\epsilon^2 = 10^{-4}$ *[*$\tau = 10^{-2}$*]:* (b) *uniform mesh,* (c) *nonuniform mesh.*

Figure 4.3(a) shows the numerical results for $\epsilon^2 = 10^{-3}$ with $\nu = 1$ at various times in a uniform mesh ($M = 1600$), while Figure 4.3(b) and (c) show the numerical results for $\epsilon^2 = 10^{-4}$ with $\nu = 10$ in uniform ($M = 1600$) and nonuniform ($M = 1348$) meshes, respectively. The nonuniform mesh is generated by DistMesh [50]. We choose larger ν for smaller ϵ^2 to control the quality of the mesh. It can be noticed that in all three cases, the mesh points will be concentrated at the thin interface after one time iteration and maintain concentrated at the moving interface all the time. The results in Figure 4.3(c) suggest that we can incorporate our Lagrangian method with an adaptive mesh technique. Within the Lagrangian solver, we only need to adapt the initial mesh. As a limitation, for this problem the Lagrangian calculation cannot reach the equilibrium, in which the circular domain disappears. Such a problem can be handled easily by applying some Eulerian solver to the numerical solutions obtained by Lagrangian calculations at the late stage.

Although we are mainly interested in the equilibrium solutions obtained by Lagrangian methods, we also compare the dynamics of the Lagrangian approach with the original Eulerian approach by studying the evolution of the diffuse interface in this example. It is well known that in the sharp interface limit, the movement of the interface is driven by mean curvature flow, and $R(t) = \sqrt{R_0^2 - 2t}$, where $R(t)$ denotes the radius of the interface at time t [68]. The singularity happens at $t = R_0/2$, which is the disappearing time. We compare the radius of the interface obtained by our numerical calculations for $\epsilon^2 = 10^{-3}$ with $R(t)$ for different choices of ν, shown in

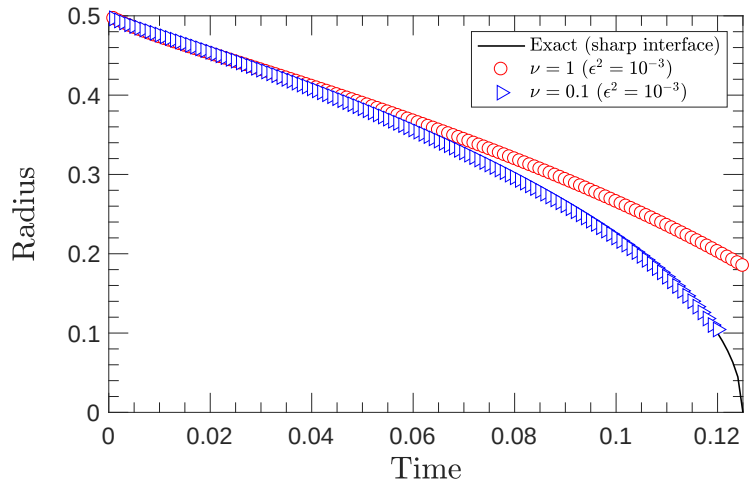

FIG. 4.4. *The evolution of the interface as a function of time by our Lagrangian method for* $\epsilon^2 = 10^{-3}$ *and different choices of* ν. *The black line show the evolution of the interface driven by mean curvature.*

Figure 4.4. We refer the readers to [68] for a similar comparison for some Eulerian methods. It can be noticed that for $\nu = 0.1$, the evolution of the sharp interface can be well approximated by our numerical solutions with a small number of mesh points. Indeed, our initial mesh size is larger than ϵ; it is impossible to get the right result by using Eulerian methods on this mesh [47]. For $\nu = 1$, it is expected that the movement of the interface is slower, similar to the previous example (see Figure 4.1(c)). Indeed, for large ν, the second term in the dissipation actually dominates the dynamics of the Lagrangian method.

4.3. Phase-field model with the volume constraint. In this subsection, we consider an Allen–Cahn type phase-field model with the volume constraint. We impose the volume constraint by introducing a penalty term in the free energy. So the total free energy of the system is given by

$$\mathcal{F} = \int_\Omega \frac{1}{2}|\nabla\phi|^2 + \frac{1}{4\epsilon^2}(\phi^2-1)^2 \mathrm{d}\boldsymbol{x} + W_b\left(\int \phi \mathrm{d}\boldsymbol{x} - A\right)^2. \tag{4.9}$$

We take $\Omega = [-1,1]^2$, $W_b = 1000$, $A = -3$, and $\epsilon^2 = 10^{-4}$ and impose the Dirichlet boundary condition $\varphi(\boldsymbol{x}) = -1, \boldsymbol{x} \in \partial\Omega$, throughout this subsection.

Figure 4.5(a) shows numerical results for the initial condition

$$\varphi_0(X,Y) = -\tanh(10(\sqrt{X^2+4Y^2} - 1/2)), \tag{4.10}$$

in which we use a nonuniform mesh ($M = 1484$) generated by DistMesh [50]. As expected, due to the effect of surface tension and the volume constraint, the bubble deforms into a circular bubble, and the mesh points remain concentrated at the thin interface when the shape of the interface changes. As a benefit of the pure Lagrangian calculation, we can guarantee the numerical solution $\varphi_h(\boldsymbol{x},t) \in [-1,1]$.

We also consider the initial condition

$$\varphi_0(X,Y) = -\sum_{i=1}^{4} \tanh(15(r_i - 1/3)) + 3, \tag{4.11}$$

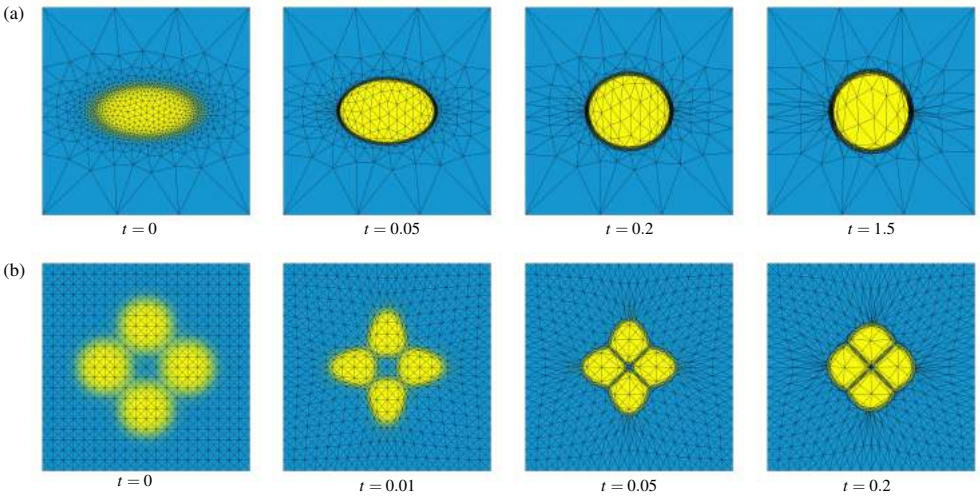

FIG. 4.5. *Numerical results for a phase-field model with the volume constrain for* $\epsilon^2 = 10^{-4}$ *with different initial conditions* ($\tau = 10^{-2}$)*:* (a) *Single bubble.* (b) *Coalescence of four kissing bubbles.*

where $r_1 = \sqrt{(X-0.4)^2 + Y^2}$, $r_2 = \sqrt{(X+0.4)^2 + Y^2}$, $r_3 = \sqrt{X^2 + (Y-0.4)^2}$, and $r_4 = \sqrt{X^2 + (Y+0.4)^2}$. This is also a classical test problem in phase-field models [41, 72], which corresponds to coalescence of four kissing bubbles. As time evolves, the four bubbles are expected to coalesce into a big bubble. The initial condition and numerical solutions obtained by the pure Lagrangian calculation at various t are shown in Figure 4.5(b) (uniform mesh, $M = 1600$). Although the mesh points are concentrated immediately at the thin diffuse interface, the nature of our Lagrangian method prevents four bubbles merging together. This is a limitation of our Lagrangian method, which cannot handle topological changes in the phase-field model, since the kinematics (2.15) is valid only locally.

This drawback can be easily overcome by running a few Eulerian steps on the obtained mesh at the reinitialization step.

A subtle issue is when we shall apply the Eulerian solver, which is problem-dependent in general. For phase-field models, the Eulerian steps are necessary to handle topological changes, like the examples in Figures 4.3 and 4.5(b). In the current study, we are not going to discuss this issue in detail. For the test problem shown in Figure 4.5(b), we actually only need one Eulerian step to handle the topological change. Figure 4.6(a) shows the numerical results with applying a Eulerian step at the fifth step ($t = 0.05$). Since we only do one Eulerian step, we didn't include the penalty term in (4.9) to ensure the maximum principle is preserved at the discrete level. Figure 4.6(b) shows the computed total discrete energy with and without the Eulerian step. It can be noticed that the Eulerian step significantly decreases the discrete energy. A better performance can be achieved by applying local mesh coarsening [7].

It is worth mentioning that for some particular problems modeled by phase-field methods, such as colloidal particles in liquid crystals [71, 73, 65], in which the coalescence of colloidal particles is often not allowed, it might be an advantage to use our Lagrangian scheme to prevent topological changes.

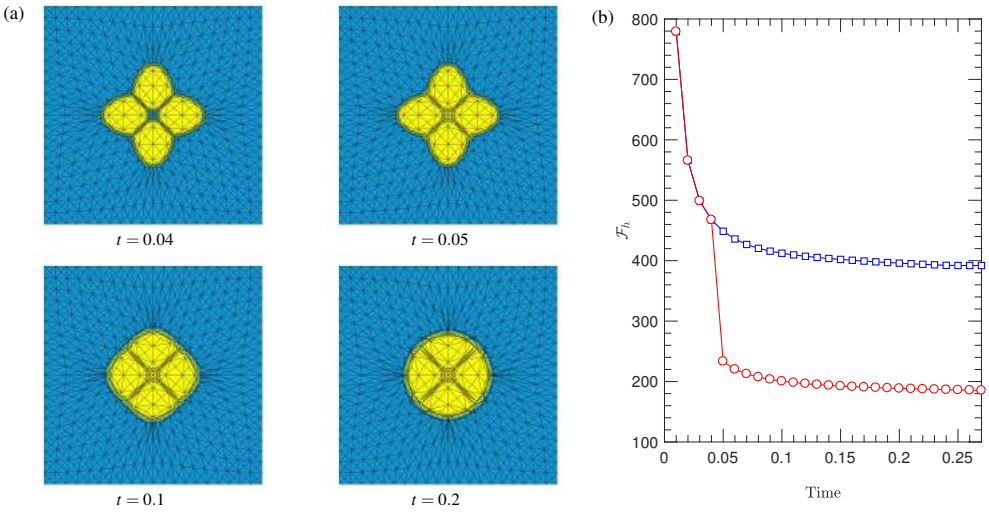

FIG. 4.6. (a) *Numerical results of "coalescence of four kissing bubbles" with an Eulerian step* ($\epsilon^2 = 10^{-4}$, $\tau = 10^{-2}$). (b) *The total discrete energy with and without the Eulerian step (blue square: Lagrangian; red circle: Lagrangian with one Eulerian step).*

4.4. "Slightly compressible" flow. In the final example, we consider a phase-field model with the total energy given by

$$\int_{\Omega_0} \frac{1}{2}|F^{-\mathrm{T}}\nabla_{\mathbf{X}}\varphi_0|^2 + \frac{1}{4\epsilon^2}(\varphi^2-1)^2 + \eta\left(\frac{1}{\det F}-1\right)^2 \det F \mathrm{d}\mathbf{X}, \tag{4.12}$$

where the last term can be viewed as a penalty term for the incompressible condition $\nabla \cdot \mathbf{u}$ in the incompressible two-phase flow [41, 38]. One can notice that this form of the free energy satisfies (3.18). This model is analogous to slightly compressible two-phase flow [60].

Figure 4.7 shows numerical results for the initial condition

$$\varphi_0(X,Y) = \max(-\tanh(15(r_1-0.7)), -\tanh(15(r_2-0.7))), \tag{4.13}$$

where $r_1 = \sqrt{X^2+4Y^2}$ and $r_2 = \sqrt{4X^2+Y^2}$, with $\epsilon^2 = 10^{-4}$ and $\nu = 10$. Here, we impose the free boundary condition on the flow map $\boldsymbol{x}(\mathbf{X},t)$ and take $\Omega_0 = [-1,1]^2$, $\epsilon^2 = 10^{-4}$, and $\eta = 5000$. As expected, the bubble will also deform into a circular bubble, and shrink. Compared with previous examples, due to the penalty term on the constrain of $\det F = 1$, the mesh will not immediately concentrate around the thin diffuse interface. One can also view the additional penalty term in the free energy as a regularization term, which improves the mesh quality.

5. Summary. In this paper, we propose a variational Lagrangian scheme to a phase-field model, which can compute equilibrium states of the original Allen–Cahn type phase-field model, with a proper choice of $\varphi_0(\mathbf{X})$. Numerical examples show that our scheme has an advantage in capturing the thin diffuse interface in equilibria with a small number of mesh points. Our approach can be extended to a general gradient flow system, especially those having equilibria with singularities, sharp interfaces, and

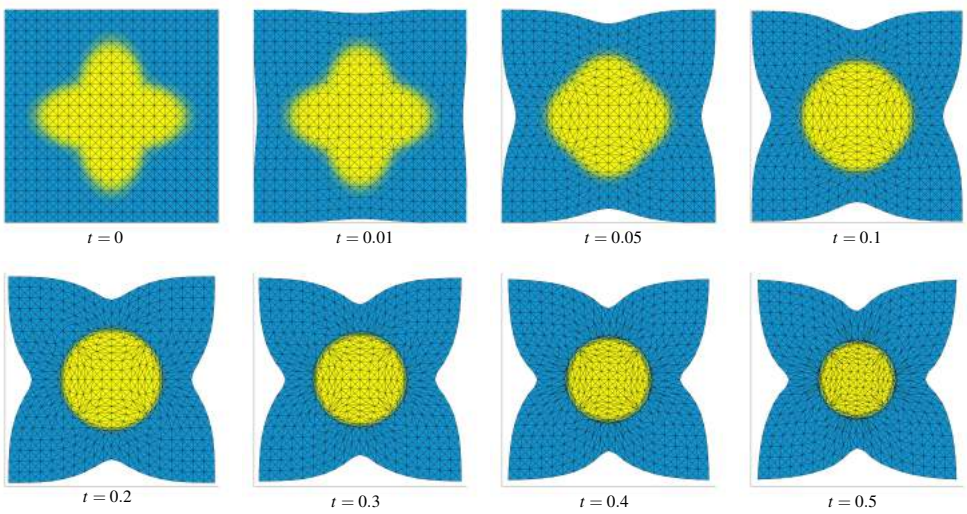

FIG. 4.7. *Numerical results for the "slightly compressible" phase-field model for* $\epsilon^2 = 10^{-4}$ $(\tau = 10^{-2})$ *at various times.*

free boundaries, such as the Landau–de Gennes model for liquid crystals [44, 66, 63] and the Ginzburg–Landau model for superconductivity [25].

There are still many limitations to our methods. As mentioned previously, it is important to combine some Eulerian solver with the Lagrangian solver presented here. For an Allen–Cahn like gradient flow system, choosing a proper initial data φ_0 is crucial in order to get a reasonable result, as the kinematic relations, i.e., the transport equation, in the Lagrangian approach may be valid only locally. Moreover, a pure Lagrangian scheme is not able to deal with large deformations and topological changes. These drawbacks might be overcome by incorporating Eulerian steps into the Lagrangian calculation. Moreover, from a numerical approximation perspective, as shown in Figure 4.2, Lagrangian methods have an advantage in capturing the interface, while Eulerian methods can achieve better numerical approximations in the bulk region. So it is necessary to combine both approaches to achieve high accuracy with small computational efforts. The main difficulty in combining a Lagrangian solver with an Eulerian solver is deciding which one to apply during the computational procedure. Another drawback for our methods, the Lagrangian mesh may still become too skewed even with the regularization term $\nu|\nabla \mathbf{u}|^2$ in the dissipation. The local mesh refinement or coarsening is needed to improve the robustness of the Lagrangian method. These points will be the subjects of future work.

Appendix A. Derivation of (2.23). In this appendix, we provide a detailed calculation of (2.23). For any smooth map $\boldsymbol{y}(\mathbf{X}, t) = \tilde{\boldsymbol{y}}(\boldsymbol{x}(\mathbf{X}, t), t)$, we denote

$$\boldsymbol{x}^\epsilon = \boldsymbol{x} + \epsilon \boldsymbol{y}, \quad F^\epsilon = \nabla_{\mathbf{X}} \boldsymbol{x}^\epsilon. \tag{A.1}$$

Then we have

$$\begin{aligned}
&\frac{\mathrm{d}}{\mathrm{d}\epsilon}\Big|_{\epsilon=0}\mathcal{F}(\boldsymbol{x}^\epsilon) = \frac{\mathrm{d}}{\mathrm{d}\epsilon}\Big|_{\epsilon=0}\left(\int_{\Omega^\epsilon} W(\varphi(\boldsymbol{x}^\epsilon), \nabla_{\boldsymbol{x}^\epsilon}\varphi(\boldsymbol{x}^\epsilon))\mathrm{d}\boldsymbol{x}^\epsilon\right)\\
&= \frac{\mathrm{d}}{\mathrm{d}\epsilon}\Big|_{\epsilon=0}\left(\int_{\Omega^0} W(\varphi_0(\mathbf{X}), (F^\epsilon)^{-\mathrm{T}}\nabla_X\varphi_0)\det F^\epsilon \mathrm{d}\mathbf{X}\right)\\
&= \int_{\Omega^0} -\left(\frac{\partial W}{\partial\nabla\varphi}\otimes\nabla_{\mathbf{X}}\varphi\right) : F^{-\mathrm{T}}(\nabla_{\mathbf{X}}\boldsymbol{y})^{\mathrm{T}}F^{-\mathrm{T}}\det F + W(\varphi,\nabla\varphi)\det F F^{-\mathrm{T}} : \nabla_{\mathbf{X}}\boldsymbol{y}\mathrm{d}\mathbf{X}\\
&= \int_{\Omega^0}\det(F)\left(-\left(\frac{\partial W}{\partial\nabla\varphi}\otimes F^{-\mathrm{T}}\nabla_X\varphi_0\right) + W(\varphi,\nabla\varphi)\mathrm{I}\right) : (\nabla_{\mathbf{X}}\boldsymbol{y}F^{-1})^{\mathrm{T}}\mathrm{d}\mathbf{X}\\
&= \int_{\Omega^0}\det(F)F^{-1}\left(-\left(\frac{\partial W}{\partial\nabla\varphi}\otimes F^{-\mathrm{T}}\nabla_X\varphi_0\right) + W(\varphi,\nabla\varphi)\mathrm{I}\right) : (\nabla_{\mathbf{X}}\boldsymbol{y})^{\mathrm{T}}\mathrm{d}\mathbf{X}.
\end{aligned}$$

Pushing forward the above result to Eulerian coordinates and performing integration by parts, we have

$$\begin{aligned}
\frac{\mathrm{d}}{\mathrm{d}\epsilon}\Big|_{\epsilon=0}\mathcal{F}(\boldsymbol{x}^\epsilon) &= \int_\Omega\left(-\left(\frac{\partial W}{\partial\nabla\varphi}\otimes\nabla\varphi\right) + W(\varphi,\nabla\varphi)\mathrm{I}\right) : \nabla\tilde{\boldsymbol{y}}\mathrm{d}\boldsymbol{x}\\
&= \int_\Omega\left(\nabla\cdot\left(\frac{\partial W}{\partial\nabla\varphi}\otimes\nabla\varphi - W(\varphi,\nabla\varphi)\mathrm{I}\right)\right)\cdot\tilde{\boldsymbol{y}}\mathrm{d}\boldsymbol{x},
\end{aligned} \tag{A.2}$$

where the boundary term vanishes due to the boundary condition of $\tilde{y}$ or φ. Hence,

$$\frac{\delta\mathcal{A}}{\delta\boldsymbol{x}} = -\frac{\delta\mathcal{F}}{\delta\boldsymbol{x}} = -\nabla\cdot\left(\left(\frac{\partial W}{\partial\nabla\varphi}\otimes\nabla\varphi\right) - W\mathrm{I}\right). \tag{A.3}$$

Appendix B. The form of the semidiscrete equation. Here we provide detailed calculations to $\frac{\delta\mathcal{A}}{\delta\Xi_i}$ and $\frac{\delta\mathcal{D}}{\delta\Xi_i'}$ in each element τ_e. The calculations are very close to the variation with respect to $\boldsymbol{x}$ and $\boldsymbol{x}_t$ in the continuous level.

Recall the discrete free energy $\mathcal{F}_h(\boldsymbol{\Xi}(t))$ and the discrete dissipation functional $\mathcal{D}_h(\boldsymbol{\Xi}(t),\boldsymbol{\Xi}'(t))$ are given by

$$\mathcal{F}_h(\boldsymbol{\Xi}(t)) = \sum_{e=1}^M\int_{\tau_e} W(\varphi_0, F_e^{-\mathrm{T}}\nabla_{\mathbf{X}}\varphi_0)\det F_e\mathrm{d}\mathbf{X} \tag{B.1}$$

and

$$\begin{aligned}
\mathcal{D}_h(\boldsymbol{\Xi}(t),\boldsymbol{\Xi}'(t)) = \frac{1}{2}\sum_{e=1}^M\int_{\tau_e}&\left|(F_e^{-\mathrm{T}}\nabla_{\mathbf{X}}\varphi_0)\cdot\left(\sum_{j=1}^N\boldsymbol{\xi}_j'\psi_j(\mathbf{X})\right)\right|^2\\
&+\nu\left|\nabla_{\mathbf{X}}\left(\sum_{j=1}^N\boldsymbol{\xi}_j'\psi_j(\mathbf{X})\right)\right|^2\det F_e\mathrm{d}\mathbf{X},
\end{aligned} \tag{B.2}$$

respectively. Let $N(i)$ be all the indices e such that $\mathbf{X}_i$ is contained in τ_e for given $\mathbf{X}_i\in\mathcal{N}_h$. Then for $\chi_i = \xi_{i,x}$ or $\xi_{i,y}$, we have

$$\begin{aligned}
\frac{\partial\mathcal{F}_h}{\partial\chi_i} &= \sum_{e\in N(i)}\int_{\tau_e}\frac{\partial}{\partial\chi_i}\left(W\left(\varphi_0(X), F_e^{-\mathrm{T}}\partial_X\varphi_0\right)\det F_e\right)\mathrm{d}X\\
&= \sum_{e\in N(i)}\int_{\tau_e} F_e^{-1}\left(\left(-\frac{\partial W}{\partial(\nabla_{\boldsymbol{x}}\varphi)}\otimes\nabla_{\mathbf{X}}\varphi_0\right)F_e^{-1} + W\mathrm{I}\right) : \left(\frac{\partial F_e}{\partial\chi_i}\right)^{\mathrm{T}}\det F_e\mathrm{d}X.
\end{aligned}$$

The numerical integration above can be computed by using the centroid method.

Meanwhile, for the dissipation part, direct computation results in

$$\frac{\partial \mathcal{D}_h}{\partial \xi'_{i,x}} = \sum_{e\in N(i)} \int_{\tau_e} \sum_{j=1}^{N} \left((\varphi_x^2 \psi_i(\mathbf{X})\psi_j(\mathbf{X}))\xi'_{j,x} + (\varphi_x\varphi_y\psi_i(\mathbf{X})\psi_j(\mathbf{X}))\xi'_{j,y}\right) + \nu(\nabla_{\mathbf{X}}\psi_i \cdot \nabla_{\mathbf{X}}\psi_j)\xi'_{i,x} \det F_e \mathrm{d}\mathbf{X} \tag{B.3}$$

and

$$\frac{\partial \mathcal{D}_h}{\partial \xi'_{i,y}} = \sum_{e\in N(i)} \int_{\tau_e} \sum_{j=1}^{N} \left((\varphi_x\varphi_y \psi_i(\mathbf{X})\psi_j(\mathbf{X}))\xi'_{j,x} + (\varphi_y^2\psi_i(\mathbf{X})\psi_j(\mathbf{X}))\xi'_{j,y}\right) + \nu(\nabla_{\mathbf{X}}\psi_i \cdot \nabla_{\mathbf{X}}\psi_j)\xi'_{i,y} \det F_e \mathrm{d}\mathbf{X}. \tag{B.4}$$

Hence,

$$\mathsf{D}(\boldsymbol{\Xi}(t)) = \mathsf{M}(\boldsymbol{\Xi}(t)) + \nu \mathsf{K}(\boldsymbol{\Xi}(\boldsymbol{t})) \tag{B.5}$$

with

$$\mathsf{M} = \begin{pmatrix} \mathsf{M}_{xx} & \mathsf{M}_{xy} \\ \mathsf{M}_{yx} & \mathsf{M}_{yy} \end{pmatrix}, \quad \mathsf{K} = \begin{pmatrix} \mathsf{K}_0 & 0 \\ 0 & \mathsf{K}_0 \end{pmatrix}.$$

Here $\mathsf{M}_{\alpha\beta}$ $(\alpha, \beta = x, y)$ is the modified mass matrix defined by

$$\mathsf{M}_{\alpha\beta}(i,j) = \sum_{e\in N(i)} \partial_\alpha\varphi(\boldsymbol{x}_e)\partial_\beta\varphi(\boldsymbol{x}_e) \det F_e \int_{\tau_e} \psi_i\psi_j \mathrm{d}\mathbf{X}, \tag{B.6}$$

where $\boldsymbol{x}_e$ is the centroid of $\boldsymbol{x}^t(\tau_e)$, and K_0 is the modified stiff matrix defined by

$$\mathsf{K}_0(i,j) = \sum_{e\in N(i)} \det F_e \int_{\tau_e} \nabla_{\mathbf{X}}\psi_i \cdot \nabla_{\mathbf{X}}\psi_j \mathrm{d}\mathbf{X}. \tag{B.7}$$

Next we show the positive definiteness of D if $\boldsymbol{\Xi} \in \mathcal{S}_{ad}^h$ and $\nu > 0$. We first show that M is positive semidefinite. Recall that M is obtained by summing the results on each element over the mesh; we only need to show $\mathsf{M}^e(\boldsymbol{\Xi})$ is positive semidefinite for each $e \in \{1, 2, \dots M\}$. The positive semidefiniteness of $\mathsf{M}^e(\boldsymbol{\Xi})$ can be proved by looking at the principal minor formed by all nonzero elements, which is a 6×6 matrix given by

$$\widetilde{\mathsf{M}}^e = \begin{pmatrix} \mathsf{M}^e_{xx} & \mathsf{M}^e_{xy} \\ \mathsf{M}^e_{xy} & \mathsf{M}^e_{yy} \end{pmatrix}, \tag{B.8}$$

where $M^e_{\alpha\beta}$ is defined by

$$M^e_{\alpha\beta} = \frac{1}{12}|\tau_e| \det F_e \left(\partial_\alpha\varphi(\boldsymbol{x}_e)\partial_\beta\varphi(\boldsymbol{x}_e)\right) \begin{pmatrix} 2 & 1 & 1 \\ 1 & 2 & 1 \\ 1 & 1 & 2 \end{pmatrix} = \partial_\alpha\varphi(\boldsymbol{x}_e)\partial_\beta\varphi(\boldsymbol{x}_e)\mathsf{M}^e_0, \tag{B.9}$$

where M^e_0 is a positive definite matrix since $\det F_e > 0$. Due to the positive definiteness of M^e_0, we can write M^e_0 as $M^e_0 = \sqrt{\mathsf{M}^e_0}\sqrt{\mathsf{M}^e_0}$. Then $\forall \mathbf{a} = (\mathbf{a}_1^{\mathrm{T}}, \mathbf{a}_2^{\mathrm{T}})^{\mathrm{T}} \in \mathbb{R}^6$ with $\mathbf{a}_i \in \mathbb{R}^3$, by direct calculation, we have

$$\mathbf{a}^{\mathrm{T}}\widetilde{\mathsf{M}}^e\mathbf{a} = \left(\partial_x\varphi(\boldsymbol{x}_e)\mathbf{a}_1^{\mathrm{T}}\sqrt{\mathsf{M}_0^e} + \partial_y\varphi(\boldsymbol{x}_e)\mathbf{a}_2^{\mathrm{T}}\sqrt{\mathsf{M}_0^e}\right)\left(\partial_x\varphi(\boldsymbol{x}_e)\sqrt{\mathsf{M}_0^e}\mathbf{a}_1 + \partial_y\varphi(\boldsymbol{x}_e)\sqrt{\mathsf{M}_0^e}\mathbf{a}_2\right)$$
$$= \left\|\partial_x\varphi(\boldsymbol{x}_e)\sqrt{\mathsf{M}_0^e}\mathbf{a}_1 + \partial_y\varphi(\boldsymbol{x}_e)\sqrt{\mathsf{M}_0^e}\mathbf{a}_2\right\|^2 \geq 0.$$

So $\widetilde{\mathsf{M}}^e$ is positive semidefinite, which indicates that $\mathsf{M}^e(\boldsymbol{\Xi})$ is positive semidefinite if $\boldsymbol{\Xi} \in \mathcal{S}_{ad}^h$. Next, we show that $\mathsf{K}(\boldsymbol{\Xi})$ is positive definite; we only need to show that $\mathsf{K}_0(\boldsymbol{\Xi})$ is positive definite, which follows the positive definiteness of the standard stiffness matrix in the finite element method. Indeed, $\forall \boldsymbol{\alpha} \in \mathbb{R}^N$,

$$\boldsymbol{\alpha}^{\mathrm{T}}\mathsf{K}_0\boldsymbol{\alpha} = \sum_{e=1}^{M}\int_{\tau_e}\left|\sum_{i=1}^{N}\alpha_i\nabla\psi_i\right|^2 \det F_e \mathrm{d}\mathbf{X} \geq c_b\int_{\Omega}\left|\nabla\left(\sum_{i=1}^{N}\alpha_i\psi_i\right)\right|^2 \geq 0,$$

where c_b is defined by $c_b = \min_{e\in\{1,2,\ldots M\}}\det F_e$, and the equality holds only if $\alpha_i = 0$, $i = 1, 2, \ldots N$. Since for $\boldsymbol{\Xi} \in \mathcal{S}_{ad}^h$, M is positive semidefinite, and K is positive definite, we can conclude that K is positive definite for $\nu > 0$. Notice that $\det \mathsf{M} = 0$, so it is important to have nonzero $\nu > 0$ to guarantee the positive definiteness of D.

Appendix C. A failed example. As mentioned previously, a pure Lagrangian calculation is sensitive to the choice of φ_0. This problem is somehow easy to deal with for the phase-field model, as it is natural to choose $\varphi_0 \in [-1, 1]$. In this appendix, we consider an extreme example by taking

$$\varphi_0(X, Y) = 2.5(X^2 - 1)(Y^2 - 1) - 1, \quad (X, Y) \in [-1, 1]^2. \tag{C.1}$$

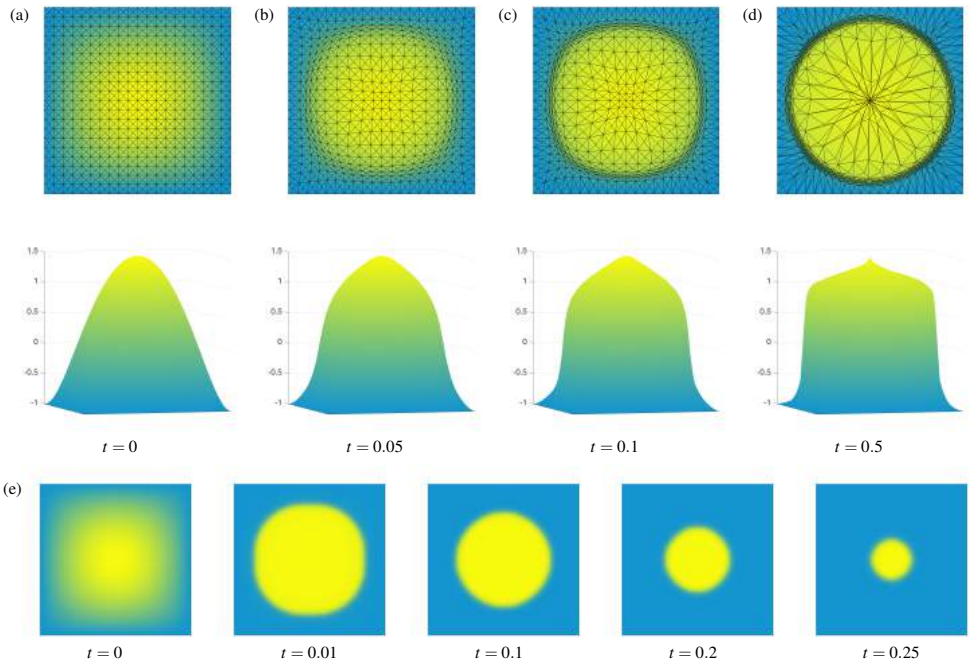

FIG. C.1. (a)–(d) *The meshes and computed solutions by the Lagrangian scheme at various times for the initial condition* (C.1) *for* $\epsilon^2 = 10^{-3}$ *and* $\nu = 10$ (*Uniform mesh.* $M = 1600$). (e) *Numerical solutions for the initial condition* (C.1) *by an Eulerian method in a uniform mesh* ($M = 64000$). *The Eulerian solver used here is the one described in section* 4.

The boundary conditions are the same as in section 4.2. Figure C.1(a)–(d) show the numerical solutions and computed meshes by our Lagrangian scheme for $\epsilon^2 = 10^{-3}$ and $\nu = 10$ at various times. Although the mesh points can be concentrated at the thin interface, the dynamics of the Lagrangian calculation is quite different with the Eulerian approach, as shown in Figure C.1(e), and fails to get the right equilibrium. With the Eulerian method, due to the discrete maximum principle, the numerical solutions will be in $[-1, 1]$ after one iteration ($\tau = 10^{-2}$). Then the bubble will deform into a circular bubble and shrink as in Figure 4.3. But in the Lagrangian approach, since the value at each mesh point cannot be changed, the only way to minimize the total energy is to minimize the size of the region with $\varphi > 1$, and the flow map will tend to be singular at $(0, 0)$, which results in a poor mesh quality at the later stage of the Lagrangian calculation.

This example illustrates the importance of a suitable φ_0. For general problems, we can use Eulerian approaches to obtain a proper φ_0, or combine Eulerian methods with Lagrangian methods in the simulation to improve the robustness of the numerical scheme.

Acknowledgment. Y. Wang would like to thank the Department of Applied Mathematics at Illinois Institute of Technology for their generous support and for a stimulating environment.

REFERENCES

[1] J. H. Adler, J. Brannick, C. Liu, T. Manteuffel, and L. Zikatanov, *First-order system least squares and the energetic variational approach for two-phase flow*, J. Comput. Phys., 230 (2011), pp. 6647–6663.

[2] S. M. Allen and J. W. Cahn, *Ground state structures in ordered binary alloys with second neighbor interactions*, Acta Metallurgica, 20 (1972), pp. 423–433.

[3] S. S. Antman, *Physically unacceptable viscous stresses*, Z. Angew. Math. Phys., 49 (1998), pp. 980–988.

[4] V. I. Arnol'd, *Mathematical Methods of Classical Mechanics*, Grad. Texts in Math. 60, Springer, New York, 2013.

[5] M. J. Baines, M. Hubbard, and P. Jimack, *A moving mesh finite element algorithm for the adaptive solution of time-dependent partial differential equations with moving boundaries*, Appl. Numer. Math., 54 (2005), pp. 450–469.

[6] J. M. Ball, *Mathematics and liquid crystals*, Molecular Crystals and Liquid Crystals, 647 (2017), pp. 1–27.

[7] R. E. Bank and J. Xu, *An algorithm for coarsening unstructured meshes*, Numer. Math., 73 (1996), pp. 1–36.

[8] A. L. Bertozzi and A. Flenner, *Diffuse interface models on graphs for classification of high dimensional data*, Multiscale Model. Simul., 10 (2012), pp. 1090–1118.

[9] C. Brett, C. M. Elliott, and A. S. Dedner, *Phase field methods for binary recovery*, in Optimization with PDE Constraints, Springer, New York, 2014, pp. 25–63.

[10] J. W. Cahn and J. E. Hilliard, *Free energy of a nonuniform system.* I. *Interfacial free energy*, J. Chem. Phys., 28 (1958), pp. 258–267.

[11] J. A. Carrillo, B. Düring, D. Matthes, and D. S. McCormick, *A lagrangian scheme for the solution of nonlinear diffusion equations using moving simplex meshes*, J. Sci. Comput., 75 (2018), pp. 1463–1499.

[12] J. A. Carrillo, Y. Huang, F. S. Patacchini, and G. Wolansky, *Numerical study of a particle method for gradient flows*, Kinet. Relat. Models, 10 (2017), pp. 613–641.

[13] J. A. Carrillo and J. S. Moll, *Numerical simulation of diffusive and aggregation phenomena in nonlinear continuity equations by evolving diffeomorphisms*, SIAM J. Sci. Comput., 31 (2009), pp. 4305–4329.

[14] J. A. Carrillo, H. Ranetbauer, and M.-T. Wolfram, *Numerical simulation of nonlinear continuity equations by evolving diffeomorphisms*, J. Comput. Phys., 327 (2016), pp. 186–202.

[15] L.-Q. Chen, *Phase-field models for microstructure evolution*, Annu. Rev. Materials Res., 32 (2002), pp. 113–140.

[16] L. Q. Chen and J. Shen, *Applications of semi-implicit Fourier-spectral method to phase field equations*, Comput. Phys. Commun., 108 (1998), pp. 147–158.
[17] Q. Cheng, C. Liu, and J. Shen, *A New Interface Capturing Method for Allen-Cahn Type Equations Based on a Flow Dynamic Approach in Lagrangian Coordinates,* I. *One-Dimensional Case*, preprint, arXiv:1911.07830, 2019.
[18] S. H. Christiansen, H. Z. Munthe-Kaas, and B. Owren, *Topics in structure-preserving discretization*, Acta Numer., 20 (2011), pp. 1–119.
[19] J. M. Church, Z. Guo, P. K. Jimack, A. Madzvamuse, K. Promislow, B. Wetton, S. M. Wise, and F. Yang, *High accuracy benchmark problems for Allen-Cahn and Cahn-Hilliard dynamics*, Commun. Comput. Phys., 26 (2019), pp. 947–972.
[20] B. Dacorogna, *A relaxation theorem and its application to the equilibrium of gases*, Arch. Ration. Mech. Anal., 77 (1981), pp. 359–386.
[21] C. M. Dafermos, *Hyperbolic Conservation Laws in Continuum Physics*, 3rd ed., Grundlehren Math. Wiss. 325, Springer, Berlin, 2005.
[22] S. R. De Groot and P. Mazur, *Non-Equilibrium Thermodynamics*, Courier Corporation, 2013.
[23] Y. Di, R. Li, and T. Tang, *A general moving mesh framework in 3D and its application for simulating the mixture of multi-phase flows*, Commun. Comput. Phys, 3 (2008), pp. 582–602.
[24] M. Doi, *Onsager's variational principle in soft matter*, J. Phys. Condensed Matter, 23 (2011), 284118.
[25] Q. Du, *Numerical approximations of the Ginzburg–Landau models for superconductivity*, J. Math. Phys., 46 (2005), 095109.
[26] Q. Du and X. Feng, *The Phase Field Method for Geometric Moving Interfaces and Their Numerical Approximations*, preprint, arXiv:1902.04924, 2019.
[27] Q. Du, C. Liu, R. Ryham, and X. Wang, *Energetic variational approaches in modeling vesicle and fluid interactions*, Phys. D, 238 (2009), pp. 923–930.
[28] B. Eisenberg, Y. Hyon, and C. Liu, *Energy variational analysis of ions in water and channels: Field theory for primitive models of complex ionic fluids*, J. Chemical Phys., 133 (2010), 104104.
[29] L. C. Evans, O. Savin, and W. Gangbo, *Diffeomorphisms and nonlinear heat flows*, SIAM J. Math. Anal., 37 (2005), pp. 737–751.
[30] J. J. Feng, C. Liu, J. Shen, and P. Yue, *An energetic variational formulation with phase field methods for interfacial dynamics of complex fluids: Advantages and challenges*, in Modeling of Soft Matter, Springer, New York, 2005, pp. 1–26.
[31] W. Feng, P. Yu, S. Hu, Z.-K. Liu, Q. Du, and L.-Q. Chen, *Spectral implementation of an adaptive moving mesh method for phase-field equations*, J. Comput. Phys., 220 (2006), pp. 498–510.
[32] X. Feng, Y. He, and C. Liu, *Analysis of finite element approximations of a phase field model for two-phase fluids*, Math. Comp., 76 (2007), pp. 539–571.
[33] D. Furihata and T. Matsuo, *Discrete Variational Derivative Method: A Structure-Preserving Numerical Method for Partial Differential Equations*, Chapman and Hall/CRC, Boca Raton, FL, 2010.
[34] M.-H. Giga, A. Kirshtein, and C. Liu, *Variational Modeling and Complex Fluids*, in Handbook of Mathematical Analysis in Mechanics of Viscous Fluids, Y. Giga and A. Novotny, eds., Springer, Berlin, 2017, pp. 1–41.
[35] O. Gonzalez and A. M. Stuart, *A First Course in Continuum Mechanics*, Cambridge University Press, Cambridge, UK, 2008.
[36] J. Hua, P. Lin, C. Liu, and Q. Wang, *Energy law preserving C0 finite element schemes for phase field models in two-phase flow computations*, J. Comput. Phys., 230 (2011), pp. 7115–7131.
[37] W. Huang and R. D. Russell, *Adaptive Moving Mesh Methods*, Appl. Math. Sci. 174, Springer, New York, 2010.
[38] Y. Hyon, D. Y. Kwak, and C. Liu, *Energetic variational approach in complex fluids: Maximum dissipation principle*, Discrete Contin. Dyn. Syst. A, 26 (2010), pp. 1291–1304.
[39] O. Junge, D. Matthes, and H. Osberger, *A fully discrete variational scheme for solving nonlinear Fokker–Planck equations in multiple space dimensions*, SIAM J. Numer. Anal., 55 (2017), pp. 419–443.
[40] C. Liu, *An introduction of elastic complex fluids: An energetic variational approach*, in Multi-Scale Phenomena in Complex Fluids: Modeling, Analysis and Numerical Simulation, World Scientific, River Edge, NJ, 2009, pp. 286–337.
[41] C. Liu and J. Shen, *A phase field model for the mixture of two incompressible fluids and its approximation by a Fourier-spectral method*, Phys. D, 179 (2003), pp. 211–228.

[42] C. Liu and Y. Wang, *On Lagrangian schemes for porous medium type generalized diffusion equations: A discrete energetic variational approach*, J. Comput. Phys., 417 (2020), 109566.
[43] C. Liu and H. Wu, *An energetic variational approach for the Cahn–Hilliard equation with dynamic boundary condition: Model derivation and mathematical analysis*, Arch. Ration. Mech. Anal., 233 (2019), pp. 167–247.
[44] C. S. MacDonald, J. A. Mackenzie, A. Ramage, and C. J. Newton, *Efficient moving mesh methods for Q-tensor models of nematic liquid crystals*, SIAM J. Sci. Comput., 37 (2015), pp. B215–B238.
[45] D. Matthes and H. Osberger, *A convergent lagrangian discretization for a nonlinear fourth-order equation*, Found. Comput. Math., 17 (2017), pp. 73–126.
[46] D. Matthes and S. Plazotta, *A variational formulation of the BDF2 method for metric gradient flows*, ESAIM Math. Model. Numer. Anal., 53 (2019), pp. 145–172.
[47] B. Merriman, J. K. Bence, and S. J. Osher, *Motion of multiple junctions: A level set approach*, J. Comput. Phys., 112 (1994), pp. 334–363.
[48] L. Onsager, *Reciprocal relations in irreversible processes.* I, Phys. Rev., 37 (1931), pp. 405–426.
[49] L. Onsager, *Reciprocal relations in irreversible processes.* II, Phys. Rev., 38 (1931), pp. 2265–2279.
[50] P.-O. Persson and G. Strang, *A simple mesh generator in MATLAB*, SIAM Rev., 46 (2004), pp. 329–345.
[51] N. Provatas, N. Goldenfeld, and J. Dantzig, *Efficient computation of dendritic microstructures using adaptive mesh refinement*, Phys. Rev. Lett., 80 (1998), pp. 3308–3311.
[52] C. Samson, L. Blanc-Féraud, G. Aubert, and J. Zerubia, *A variational model for image classification and restoration*, IEEE Trans. Pattern Anal. Machine Intell., 22 (2000), pp. 460–472.
[53] R. Schoen and K. Uhlenbeck, *A regularity theory for harmonic maps*, J. Differential Geom., 17 (1982), pp. 307–335.
[54] J. Shen, *Modeling and numerical approximation of two-phase incompressible flows by a phase-field approach*, in Multiscale Modeling and Analysis for Materials Simulation, World Scientific, River Edge, NJ, 2012, pp. 147–195.
[55] J. Shen, J. Xu, and J. Yang, *A new class of efficient and robust energy stable schemes for gradient flows*, SIAM Rev., 61 (2019), pp. 474–506.
[56] J. Shen and X. Yang, *An efficient moving mesh spectral method for the phase-field model of two-phase flows*, J. Comput. Phys., 228 (2009), pp. 2978–2992.
[57] W. Strutt, *Some general theorems relating to vibrations*, Proc. Lond. Math. Soc., 1 (1871), pp. 357–368.
[58] M. Sulman, J. Williams, and R. D. Russell, *Optimal mass transport for higher dimensional adaptive grid generation*, J. Comput. Phys., 230 (2011), pp. 3302–3330.
[59] H. Sun and C. Liu, *On energetic variational approaches in modeling the nematic liquid crystal flows*, Discrete Contin. Dyn. Syst., 23 (2009), pp. 455–475.
[60] R. Temam, *Navier-Stokes Equations: Theory and Numerical Analysis*, AMS, Providence, RI, 2001.
[61] R. Temam and A. Miranville, *Mathematical Modeling in Continuum Mechanics*, Cambridge University Press, Cambridge, UK, 2005.
[62] S. O. Unverdi and G. Tryggvason, *A front-tracking method for viscous, incompressible, multi-fluid flows*, J. Comput. Phys., 100 (1992), pp. 25–37.
[63] Y. Wang, G. Canevari, and A. Majumdar, *Order reconstruction for nematics on squares with isotropic inclusions: A Landau–De Gennes study*, SIAM J. Appl. Math., 79 (2019), pp. 1314–1340.
[64] Y. Wang, C. Liu, P. Liu, and B. Eisenberg, *Field Theory of Reaction-diffusion: Mass Action with an Energetic Variational Approach*, preprint, arXiv:2001.10149, 2020.
[65] Y. Wang, P. Zhang, and J. Z. Chen, *Formation of three-dimensional colloidal crystals in a nematic liquid crystal*, Soft Matter, 14 (2018), pp. 6756–6766.
[66] Y. Wang, P. Zhang, and J. Z. Y. Chen, *Topological defects in an unconfined nematic fluid induced by single and double spherical colloidal particles*, Phys. Rev. E, 96 (2017), p. 042702.
[67] M. Westdickenberg and J. Wilkening, *Variational particle schemes for the porous medium equation and for the system of isentropic Euler equations*, ESAIM Math. Model. Numer. Anal., 44 (2010), pp. 133–166.
[68] J. Xu, Y. Li, S. Wu, and A. Bousquet, *On the stability and accuracy of partially and fully implicit schemes for phase field modeling*, Comput. Methods Appl. Mech. Engrg., 345 (2019), pp. 826–853.

[69] X. Xu, Y. Di, and M. Doi, *Variational method for liquids moving on a substrate*, Phys. Fluids, 28 (2016), 087101.
[70] J. Yin, Y. Wang, J. Z. Y. Chen, P. Zhang, and L. Zhang, *Construction of a pathway map on a complicated energy landscape*, Phys. Rev. Lett., 124 (2020), 090601, https://doi.org/10.1103/PhysRevLett.124.090601.
[71] P. Yue, J. J. Feng, C. Liu, and J. Shen, *A diffuse-interface method for simulating two-phase flows of complex fluids*, J. Fluid Mech., 515 (2004), pp. 293–317.
[72] Z. Zhang and H. Tang, *An adaptive phase field method for the mixture of two incompressible fluids*, Comput. & Fluids, 36 (2007), pp. 1307–1318.
[73] C. Zhou, P. Yue, and J. J. Feng, *Dynamic simulation of droplet interaction and self-assembly in a nematic liquid crystal*, Langmuir, 24 (2008), pp. 3099–3110.